CHALMERS
UNIVERSITY OF TECHNOLOGY

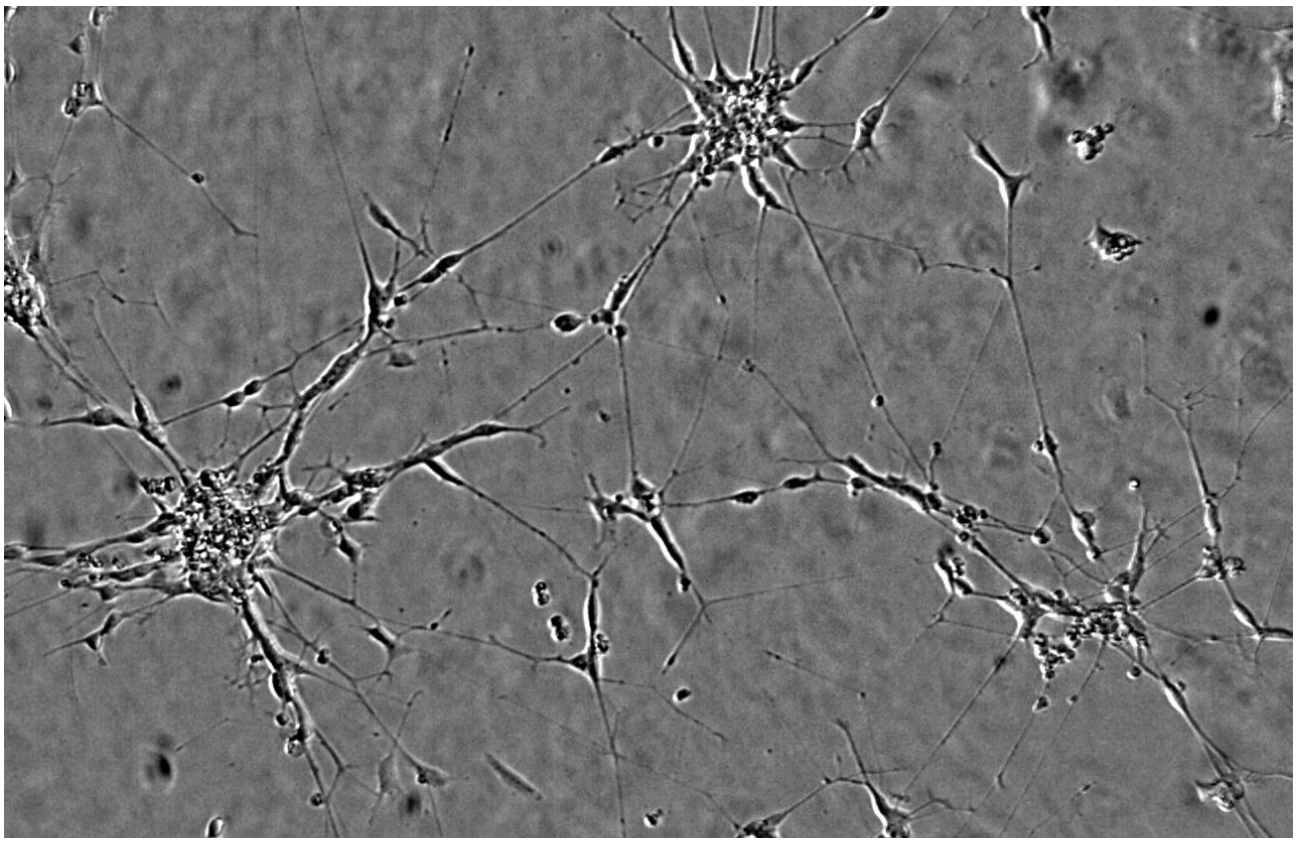

Development of a 3D in-vitro model for Alzheimer's disease:

Behavioral investigation of SH-SY5Y cells in brain-mimicking matrices.

Master's thesis in Biomedical Engineering

ERIK HARDSELIUS

Department of Biology and Biological Engineering
CHALMERS UNIVERSITY OF TECHNOLOGY
Gothenburg, Sweden 2017

Development of a 3D in-vitro model for Alzheimer's disease:

Behavioral investigation of SH-SY5Y cells in brain-mimicking matrices.

Master's thesis in Biomedical Engineering

ERIK HARDSELIUS

SUPERVISOR
Nisha Rani Agarwal
Chalmers University of Technology, Gothenburg

EXAMINER
Pernilla Wittung Stafshede
Chalmers University of Technology, Gothenburg

Department of Biology and Biological Engineering
Chalmers University of Technology
SE-412 96 Göteborg
Sweden
Telephone + 46 (0)31-772 1000

Development of a 3D in-vitro model for Alzheimer's disease:

Behavioral investigation of SH-SY5Y cells in brain-mimicking matrices.

Master's thesis in Biomedical Engineering

ERIK HARDSELIUS

Department of Biology and Biological Engineering
Chalmers University of Technology
SE-412 96 Göteborg
Sweden
Telephone + 46 (0)31-772 1000

Cover:
Brightfield of Neuronal Differentiated SH-SY5Y cells in Glycidyl Methacrylated Hyalronic acid brain model displaying neurite-like growths after two weeks in culture.

Development of a 3D in-vitro model for Alzheimer's disease:

Behavioral investigation of SH-SY5Y cells in brain-mimicking matrices.

Master's thesis in Biomedical Engineering

Chalmers University of Technology

Abstract

Worldwide over 50 million people are suffering from Dementia and 60-70% of these cases are believed to be linked to Alzheimer's disease (AD) (*1*). Studies show that people suffering from repeated or severe head trauma (*2*), such as professional boxer's, and people with Down's syndrome(*3*, *4*) are more prone to develop Alzheimer's disease later in life. One common feature in these medical cases is an altered extracellular matrix in the brain due to either trauma or genetic factors. Understanding the mechanisms behind AD have has proven a challenge to the scientific community due to the lack of a functional disease model for AD. So far, the full AD progression has yet to be adequately modelled in a controlled setting, such as an *in vitro* or *in vivo* model, even though at least one promising candidate has been reported by Choi *et al*. utilizing 3D-cell culturing system that displays increased levels of both intracellular phosphorylated-tau proteins and extracellular amyloid β plaques compared to a 2D control (*5*).

In this work a bare bones tuneable brain 3D-cell model protocol is presented and evaluated using three different cell lines of differentiated SH-SY5Y neuroblastoma cells. The most promising conditions in the matrix show neuron-like cells that exhibit comparable morphology to those presented by previous models but in a more controlled and well defined environment. The model makes promising use of hyaluronic acid in a 3D-matrix seeded with differentiated cells. Studies performed in the new model hints towards an ultimately cytotoxic interaction between Aβ and ECM components, which encourages further investigations of neuron/ECM/Aβ interactions in AD.

Keywords: SH-SY5Y, 3D-cell model, neuronal differentiation, hyaluronic acid, collagen, hydrogel, microscopy

Abbreviations

AA - Acetic Acid

Aβ - Amyloid β

AD - Alzheimer's disease

APP - Amyloid Precursor Protein

BME - Brain Mimicking Environment

Col-I - Collagen type 1

ECM - Extra Cellular Matrix

EthD – Ethidium Homodimer

GM - Glycidyl Methacrylate

GMHA - Glycidyl Methacrylate Hyaluronic Acid

HA - Hyaluronic Acid

HCL - Hydrochloric acid

LD - Live/Dead assay

MPM - Multi Photon Microscopy

MDS - Meso Scale Discovery Human (6E10) Abeta Triplex Assay

SPM - Single Photon Microscopy

SHG - Second Harmonics Generation

Acknowledgement

There are many people to whom thanks are due and I wish to begin by thanking my supervisor Nisha Rani Agarwal for her support and Stéphanie Blockhuys for her supervision during the first half of the project. I wish to extend a big thanks the people of the molmic group: Juris Kiskis, in loving memory, for his constant questions and our many discussions. Alexandra Paul for pushing me to finish and for always being ready to help with things big and small. Mikael Stuhrenberg for the gaming discussions. Arsalan for sharing many hours in the Master room with me. I also wish to thank the many wonderful people at Sahlgrenska: Lotta Agholme, Petra Bergström and Henrik Zetterberg, for their expertise and assistance. Then I would like to send out a special thanks to my friends and family, for putting up with me during this long year. Lastly I wish to thank my examiner, Pernilla Wittung Stafshede.

Table of Contents

Figures

Tables

1. Introduction

1.1 Why Alzheimer's Disease?

Worldwide over 50 million people are suffering from Dementia and 60-70% of these cases are believed to be linked to Alzheimer's disease (AD) (*1*). Studies show that people suffering from repeated or severe head trauma, such as professional boxers (*2*) and people with Down's syndrome (DS) (*3*, *4*) are more prone to develop Alzheimer's disease later in life. One common feature in these medical cases is the increased presence of fibrous extra-cellular components in the brain such as collagen. In the case of boxing the presence of collagen is related to tissue scar formation (*6*, *7*) from repeated head trauma and in the case of Down's patients it is a consequence of the genetic upregulation of collagen and amyloid precursor protein (APP) production. The genes for the two proteins are linked as they are both present on the extra copy of chromosome 21 (*3*).

Understanding the mechanisms behind AD has proven a challenge for the scientific community due to the lack of a functional disease model mimicking all stages of the complex developmental stages of the disease. There are two distinct pathological hallmarks of AD: (i) The formation of extracellular amyloid plaques derived from amyloid β (Aβ) peptides created by the cleavage of APP and (ii) the intracellular neurofibrillary tangles composed of filamentous aggregations of phosphorylated-tau proteins (p-tau) (*8*). These two hallmarks have yet to be linked together in a single hypothesis. The most widely accepted hypothesis of the cause of AD, the amyloid hypothesis, stipulates that Aβ accumulates and aggregates in the extracellular matrix (ECM) causing the formation of plaques interfering with the neurites, leading to synaptic dysfunction and eventually cell death. While according to the tau hypothesis the main factor is instead abnormal or excessive phosphorylation of the intracellular tau, leading to development of paired helical filament tau that form neurofibrillary tangles interfering with the intracellular functions of the neurons, such as cytoplasmic functions and axonal transport (*9*). So far, the full AD progression has yet to be adequately modelled in a controlled setting, such as an *in vitro* model, even though at least one promising candidate has been reported by Choi *et al*. utilizing 3D-cell culturing system that displays increased levels of both p-tau and Aβ compared to a 2D control (*5*).

1.2 Alzheimer's

In order to understand AD, it is important to understand the normal role of the proteins involved in the disease. The main focus here has to be put on APP, due to its role in the formation of Aβ- plaques that is the main hallmark of AD. APP is a cell surface protein that when incorrectly cleaved by β- and γ-secretase release short protein fragments, among others different lengths of Aβ (*10*). Some of these fragments, chief among them Aβ42 are 'sticky' and bundle up in the extracellular space into plaques, referred to as Aβ-plaques, that are believed to interfere with normal neuron activity (*10*) even though the pre-plaque oligomers have been suspected as an even bigger factor in neuronal damage then the plaques themselves. The non-pathological role of the full APP unfortunately, has not been subject to many studies until recent years and the actual role of the protein is still contested and defined more of what it does not do, then its intrinsic function. Recent studies performed with APP-knockout mice reached no clear conclusion other than involvement with the natural development of the nervous system (*11*). Previous studies (*12*) on null-APP mice models shoved that mice not expressing APP had, on the surface, normal looking synaptic development, despite exhibiting severe learning difficulties and therefore that the protein has some, albeit unknown, function is clear.

1.2.1 Alzheimer's disease symptoms

AD is a chronic disease associated with age and one of the diseases referred to, along Parkinson's and others, as dementia (*13*). AD is a slow-working disease and generally, the first symptom to appear is gradual impairment in episodic memory. This loss of memory or inability in recollection cannot be improved significantly by training, reminders or memory techniques (*14*). As the disease progresses the patient need more and more assistance with increasingly rudimentary tasks until at the final stages of the disease the person is completely unable to fend for themselves AD causes symptoms of dementia such as memory loss, difficulty performing daily activities, and changes in judgement, reasoning, behaviour and emotions. These dementia symptoms are irreversible, which means that any loss of abilities cannot be gained back with current standards in medical treatment (*14*). The progress of the disease is continuous but for ease of diagnosis a scale has been developed in order to

determine the severity of the disease and how much assistance is required by the caregiver as presented in Table 1.

TABLE 1 THE GLOBAL DETERIORATION SCALE (*13*).

The Global Deterioration Scale (GDS)	
Stage of the disease	**Symptoms**
Stage 1: Normal function)	- No symptoms
Stage 2: Very mild cognitive decline (could be normal age related changes or earliest signs of AD)	- Small Memory lapses - Forgetting familiar names and locations of objects - Not especially noticeable to others
Stage 3: Mild cognitive decline (diagnosis of early stage AD possible in some, but not all individuals with these symptoms)	- Mild forgetfulness - Difficulty learning new things - Difficulty concentrating or limited attention span - Problems with orientation, such as getting lost - Communication difficulties such as finding the right word - Loss or misplacing of valuable objects - Difficulty handling problems at work - Issues are noticeable to family, friends or co-workers
Stage 4: Moderate cognitive decline (early stage or mild AD)	- Some memory loss of personal history - Difficulty with managing complex tasks e.g., managing finances, shopping, travel - Decreased knowledge of both current events and recent events - Impaired ability to perform challenging mental arithmetic (such as counting backward from 83 by increments of 7)
Stage 5: Moderately severe cognitive decline (mid-stage or moderate AD)	- Major gaps in memory, forgetting phone numbers or names of close family members - Help is needed with day-to-day tasks
Stage 6: Severe cognitive decline (mid-stage or moderately severe AD)	- Continued memory loss, occasionally forgetting the name of a spouse or primary caregiver - Loss of awareness of recent events and experiences in their lives, such as what dinner they just had - Assistance is needed with activities of daily living e.g., getting dressed, bathing - Difficulties counting - Personality and emotional changes such as confusion, anxiety, suspiciousness, anger, sadness/depression, hostility, apprehension, delusions and agitation - Obsessions such as repetition of simple activities - Disruption of normal sleep/waking cycle - Increasing episodes of incontinence
Stage 7: Very severe cognitive decline (late-stage or severe AD)	- Severe cognitive impairment - Vocabulary becomes limited and eventual loss of speech - Loss of ability to walk independently and sit without support - Help is needed with basic tasks such as eating and using the toilet - usually incontinent

1.2.2 Neuropathological hallmarks of Alzheimers

The major neuropathological hallmarks of AD are neuronal loss, neurofibrillary degeneration and Aβ deposition in extracellular neuritic plaques and in the wall of brain vessels (*9*, *15*). The degeneration of the neurons causes the brain to suffer from atrophy; essentially the brain wastes away, Figure 1, losing function over time. The cause

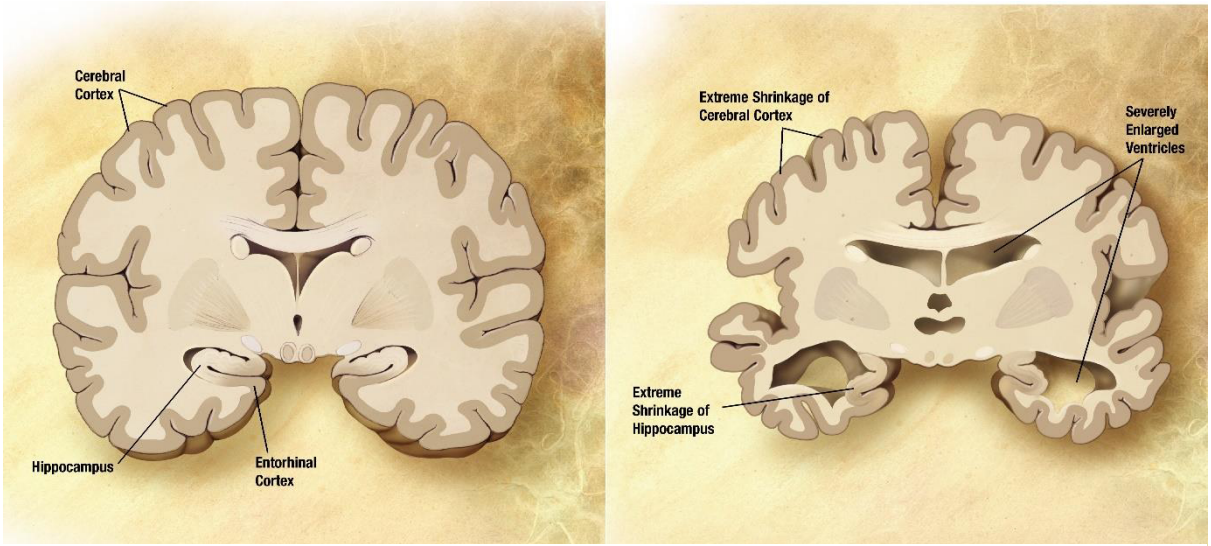

FIGURE 1 A COMPARISON OF AN HEALTHY BRAIN (LEFT) AND A BRAIN SUFFERING FROM ALZHEIMER'S DISEASE (RIGHT) (*51*)

of this neurofibrillary degeneration is hypothesised to be a combination of toxic Aβ peptide species in both the extracellular and intracellular environment and p-tau protein species interfering with internal cell functions (*14*). There is no known cure for Alzheimer's and no known way to restore lost neural function or abilities' that has been lost due to the disease (*13*).

1.3 Alzheimer's disease and Down's syndrome

Aβ is derived from APP and the gene coding for APP is located on the long arm on chromosome 21 (*15*). In Down's syndrome or trisomy 21, there is an extra copy of this chromosome and therefore an extra copy of the APP gene which leads to an overexpression of APP in the adult brain (*16*). The same chromosome is also linked to the expression of hyaluronic acid (HA) and collagen, which are key components in the extracellular matrix (ECM) in the body (*17*). HA in particular is combined with different proteoglycans of the lectican family as well as glycoproteins from the tenascin family to form the majority of the ECM of the brain (*17*, *18*). The majority of neurons in the cortex and subcortical in all humans during early childhood are Aβ positive, and the distribution of Aβ acquired during late childhood is retained during adulthood (*15*). The stable distribution of Aβ during most of the lifespan of an average human, not afflicted with any neuronal pathology, suggests that the presence, or even abundance, of Aβ in neurons, is in itself not sufficient to explain AD. This suggests alternative or complementary factors leading to the formation of the extracellular neuritic plaques need to be considered (*15*). Further weight to the argument that Aβ is not the sole culprit stems from studies performed on people with DS of different ages. Apart from the *intracellular* Aβ, many people with DS have a unique brain feature that has been found in a broad age spectrum of people with DS. They exhibit extracellular plaques formed from Aβ, yet these are amorphous, diffuse, non-fibrillar and seems to have either negligible, or no adverse effects on neurons, nor observable clinical consequence due to their deposition (*19–21*). The study in question spanned people ranging from 35 to as early as from 8 years of age at which time no cases of AD was found (*19*, *22*). Further complicating the issue is a subset of the DS population that despite having the clinical hallmarks of AD pathology do not appear to develop clinical signs of dementia at any age (*21*). Despite these conflicting issues regarding APP, plaques and Alzheimer's, of people with DS reaching the age of 60, the dementia rate is between 15-77% and DS remains closely affiliated with AD (*21*).

1.4 Alzheimer's disease and Head trauma

Several studies link head injuries to increased risks or a quick progression of AD(*2*, *7*, *23–25*). These studies list different reasons that might correlate to this increase, such as an increased APP-production as a response to the injury, as well as a compromised blood brain barrier due to ruptured microvasculature depositing non-native ECM components in the brain(*7*, *25*). One study in particular claims a doubling of the risk of developing the disease due to medium or severe head trauma (*24*). Hashimoto *et al.* (*26*) found in 2002 that a connection between ECM components and amyloid plaques by identifying a collagen-like component, found inside the characteristic plaques of a brain suffering from AD (*26*).

1.5 State of the art

Several AD models have been developed with focus on different aspects of the disease. Some are systematic models such as the null and knockout APP mice models mentioned earlier (*11*, *12*) others are in vitro cell models. The biggest issue with these *in vivo* models compared to *in vitro* are the same as with studying AD patients, in that it is hard to investigate the molecular interactions while they happen, and problems in with rampant cost for large scale studies. This challenge is both due to ethical considerations and the technical issue accessing the brain in a living creature which makes these studies both very expensive and time consuming to perform. Other challenges with in vivo studies are the abundance of factors present in a living system that makes conclusions about the effects of single chemicals and proteins difficult to draw. Even so, there are clear advantages of the systematic approach effects on higher functions such memory, behaviour and learning are impossible to study in a dish, as of yet and the different models complement each other.

In order to study the basic interactions between ECM, APP and neurons, special interest has been given to the following in vitro cell models:

(i) A model using differentiated APP-producing SH-SY5Y grown in Matrigel developed by Agholme *et al.* in 2010, has been used to study intercellular APP in neurons (*27*). The study focused in particular on the transportation of excess APP and its derivatives between neurons, using axonal transportation, showing the use of cell lines in the study of AD (*27*). (ii) Suri *et al.* have developed an HA based model for 3D-growth of Schwan cells for long term studies showing increased production of neurotropic factors and the possibility of custom 3D matrixes using ECM components present in the brain (*28*). (iii) Choi et al. have demonstrated plaque and tangle pathology formation in neurites after 6 weeks in a 3D-Matrigel environment using immortalised human derived neuron progenitor cells (*5*).

1.6 Motivation of study

The purpose of the herein presented study is to create a fully reproducible 3D-model to perform basic studies of cellular mechanisms in AD by combining facets from the models created by Suri *at al* and Agholme *at al*.

The Matrigel used in the models(*27–29*) is a commercially available natural extract product that is used specifically to support cells in both 3D and 2D cell culture. Matrigel contains numerous growth factors and components (*30*) that while very useful to grow neurons in makes it difficult to research the effects of single ECM components. The effect different ratios of the growth factors on the neurons grown in the gel becomes difficult to isolate. Batch to batch variety in presence and ratios of these components is also an issue that is not easily addressed as each batch would need to be thoroughly investigated before use which would be both time and resource consuming.

Therefore the aim of the current study is to create a novel *in vitro* brain model of AD, consisting of known basic components in order to examine the effects of the ECM itself on potential disease progression and neuron growth. The study consists of the establishment of a 3D-ECM hydrogel focused concept, seeded with neuronal differentiated SH-SY5Y cells expressing APP using neuronal differentiated wild type of the same cell line as a control. The model is then to be evaluated on the neuronal morphology of the cells and expression of APP in media as they grow in the gels during a 6-week period, to establish the potential for use as an Alzheimer's model.

2. Materials and Method

2.1 Synthesis of Glycidyl Methacrylate Hyaluronic Acid

The gels that form the basis of the model was prepared in the following way based on a protocol used by Suri *et al.*(*28*). First Glycidyl Methacrylate Hyaluronic acid (GMHA) was synthesised from commercially available Hyaluronic Acid (HA, 120K15211V, Sigma) and Glycidyl Methacrylate (GM, A0355103, ACROS), whose chemical structure is presented in Figure 2. The HA was dissolved to a 1% w/v solution in milliQ water in a beaker that was sealed using parafilm and the contents subsequently stirred overnight into a homogenous fluid. Next a 20-fold molar excess of Triethylamine (S7047452526, Millipore) was added to the beaker in order to facilitate the bonding of the GM to the HA and the solution was stirred for 10 minutes to make it homogenous. Finally, a 20-fold molar excess of GM was added and the solution stirred overnight once more.

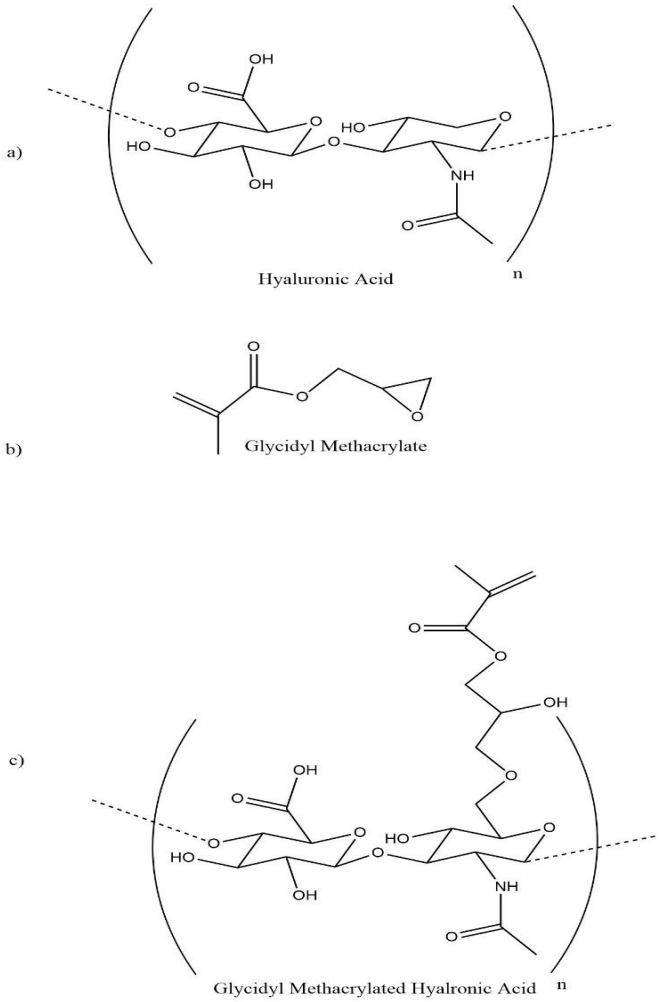

FIGURE 2 CHEMICAL REPRESENTATION OF A) HYALURONIC ACID POLYMER, B) GLYCIDYL METHACRYLATE, AND C) GLYCIDYL METHACRYLATE HYALURONIC ACID (24). IMAGE CREATED IN CHEMDRAW 2016

The GMHA in the solution was purified from the Triethylamine by Aceton precipitation (Pierce, 2007). First the GMHA solution was mixed in a 1:4 ratio with -20 ℃ Aceton in a centrifuge proof Falcon-tube and vortexed for 1 minute to homogenize the solution. The solution was then placed in the freezer at -20 ℃ for 1 hour. Next, the -20 ℃ GMHA solution was spun in a 4℃ centrifuge for 10 minutes at 13 000 g to gather the GMHA in the bottom of the falcon tube in the form of a pellet. Afterwards the supernatant was gently decanted from the falcon tube and the pellet was left to air-dry for 5 minutes after which it is resuspended in a small volume of milliQ water and the Aceton precipitation process repeated.

After a total of two precipitation runs, the GMHA pellet was resuspended in milliQ water and placed in a -80 ℃ freezer to completely solidify. The tube containing the GMHA ice, was placed in a vacuum freeze dryer and kept

until all ice had been removed, see Figure 3. Lastly the GMHA was placed in the dark in a desiccator at room temperature for 1 day to remove excess moisture and then stored in the dark in -20 ℃.

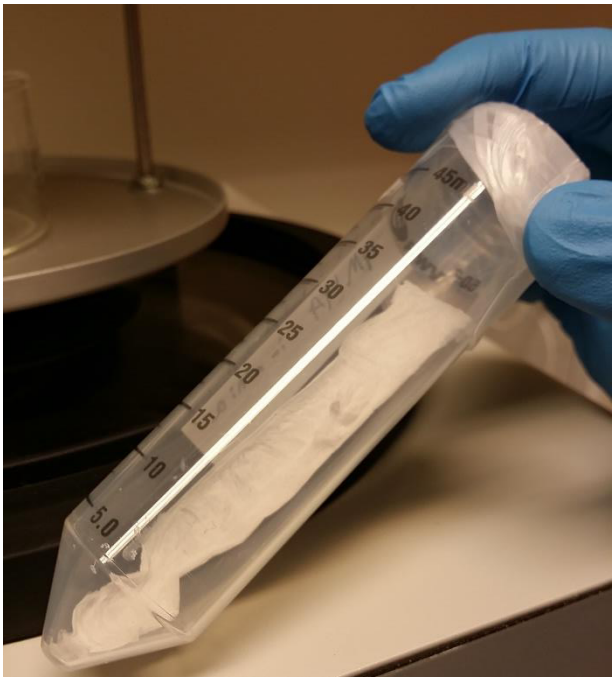

FIGURE 3 GMHA AFTER COMPLETING FREEZE DRYING PROCESS.

2.2 HEPES+ Buffer solution preparation

The second step of the brain mimicking environment (BME) synthesis process was to prepare the buffer solution.

The buffer solution is a mix consisting of HEPES and Sodium Bicarbonate dissolved in milliQ water and pH adjusted to 7.2 using Hydrochloric Acid (HCL). This adjustment is done both at creation and again before inclusion in the BME-matrix. The buffer was selected for three reasons, first, it was used in order to kick-start the fibrillation of the Col-I by neutralizing the Acetic acid used as a dilution agent in the Col-I stock solution and thus bringing the pH up to a range where fibrillation is favourable. Second, it was used to bring the pH of the matrix into the physiological range of pH ~7 in order to make the local matrix environment viable for the SH-SY5Y cells. Third, it was used to adjust the osmolarity of the BME-matrix to physical relevance (*31*).

2.3 Collagen dilution

The collagen was diluted to the required concentration using 0.2% Acetic Acid (AA). The concentration of Col-I in the final gel was varied between 0.5 mg/ml to 3 mg/ml. Comparison studies between different concentrations of collagen were done using SHG.

2.4 Incubation time

The incubation time of the uncrosslinked hydrogel was varied between 1H and 24H and size and distribution of fibrils and general matrix structure was investigated using SHG. The viability of cells was determined by observing the morphology and using live/dead-staining.

2.5 Cell lines

This study was performed using three different cell lines SH-SY5Y, SH-SY5Y APP-overexpressing and SH-SY5Y Vector control. The third cell line serves as a control for the transfection procedure while the first and second mimic normal brain APP-function and DS-brain function respectively.

All cell lines possess differentiation capability towards neuron-like morphology by means of a retinoic acid differentiation protocol.

SH-SY5Y is a subcloned cell line taken from the cell line SK-N-SH, which is of human neroblastoma origin(*32*). SK-N-SH itself is derived from a bone marrow biopsy of a 4-year old girl and first reported in 1973 and has been widely used since then(*33*). SH-SY5Y cells are most often used as an in vitro model of differentiation and neuronal function, and have been used to study neuronal diseases such as Parkinson's Disease(*34*).

The SH-SY5Y APP overexpressing variant donated by Agholme *et al.* had already been treated with a gene transfection using the pcDNA3.1 vector with which APP695 cDNA(wild type) had been inserted into the SH-SY5Y using FuGene 6 transfection agent(Roche, Basel, Switzerland). Stably transfected cells had been ensured by using the antibiotic G418 (500 g/ml; Invitrogen, Paisley, UK) and verified by using western blotting. The Vector control had been subjected to the same treatment without APP695 cDNA inside the vector.

The SH-SY5Y vector control was also generously provided by Agholme *et al.*

2.6 Cell Culturing

The cell lines where cultured in a base media of Dulbecco's Modified Eagles Medium/F12 + Glutamax (1xDMEM, 1715888, Gibco) containing 10% Fetal Bovine Serum (FBS, AXK51176, HyClone) and 1% Penicillin and Streptomycin (PEST, 34146, Fisher BioReagents) and grown in tissue culture-treated T25 flasks(VWR) in a humid atmosphere at 37℃ and 5% CO_2.

The cells were grown to about 80-90 % confluency before being split in 1:4 ratio for the undifferentiated cell lines and 1:10 during RA-differentiation. The cell media was changed the day after bringing any cells into culture, and then 2 times a week after that, until cells where used in experiments. For neuron pre-differentiation, 10µM Retinoic Acid was added to the base media and the cells were in differentiation for between 7-11 days before being used in experiments. The media used with the APP-overexpressing and APP-vector control cells were supplemented with 0.8% G418(13811200, Roche) to select for stably transfected cells until the cells were used in experiment.

For the in matrix neuronal differentiation experiments performed in the model, serum-free base media with 0.1mM Brain derived neurotropic factor (BDNF, #051461, Peprotech) was used for all conditions.

For cell seeding, TrypLe Express (1713951, Gibco) was used for cell detachment and DPBS (1553601, Gibco) for cell washing. Cell counting was done using a Neuberger haemocytometer.

2.7 3D-matrix preparation

The process of creating the matrix is summarized below in Figure 4. The crosslinker Irgacure 2959 (0014016263, BASF), was dissolved in PBS and used at a final concentration of 1% (w/v) in the gels together with 2% (w/v) GMHA. This mixture was then vortexed for 2 minutes and then placed in a shaker at 800 rpm overnight in order to achieve a homogenous fluid.

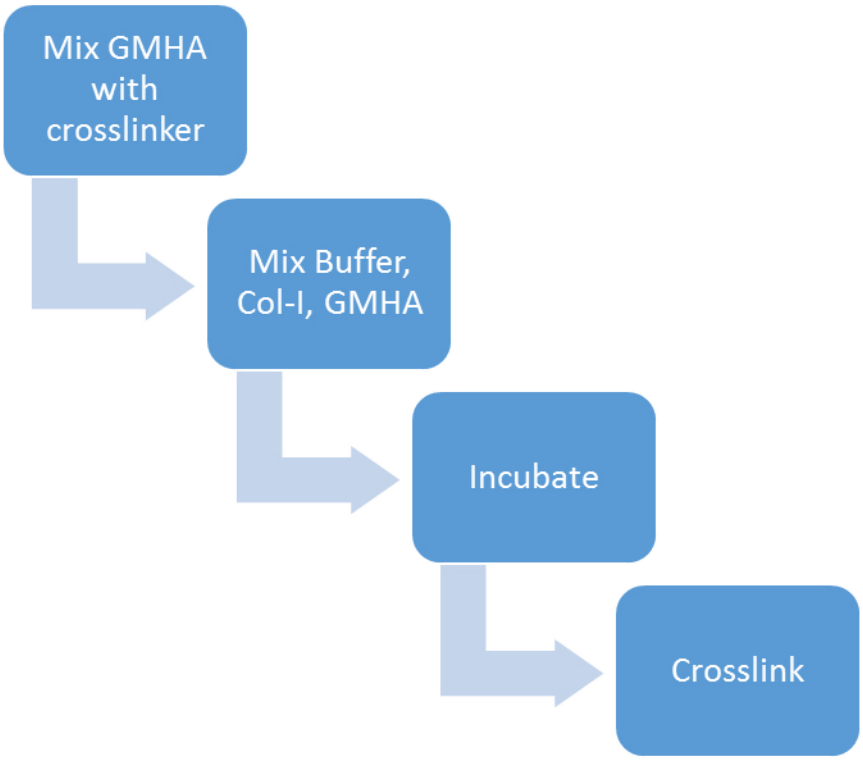

FIGURE 4 3D MATRIX PREPARATION

The next step was performed working on ice inside the sterile hood. The GMHA mixture was mixed with an equal part of Human Collagen-I 3.2mg/ml (7292, VitroCol) solution, pre-diluted using Acetic acid to reach the desired concentration. Gentle pipetting was used to mix the two fluids thoroughly together.

Next, the cell media was mixed with an equal part of the buffer solution by gentle pipetting. The buffer solution was a mix consisting of HEPES (A0368514, ACROS) and Sodium Bicarbonate (A0366538, ACROS) dissolved in milliQ water and pH adjusted to ~7.2 using 2M Hydrochloric Acid (HCL). In cell experiments the cells was prepared and present in the cell media, 6000 cells/µl final gel concentration. The contents of the media were adapted to the specific cell type.

The GMHA-Col-I solution was then in turn mixed with the buffer solution by gentle pipetting, resulting in an uncrosslinked hydrogel with or without cells present depending on the experiment. The ratios between the solutions of Col-I, GMHA, Buffer/cell media was kept to 4:4:2 as shown in Figure 5. The hydrogel mix was then pipetted gently using reversed pipetting into the wells of 1.5 Glass bottom 96-well plate (Cellvis). The 30 µl gels

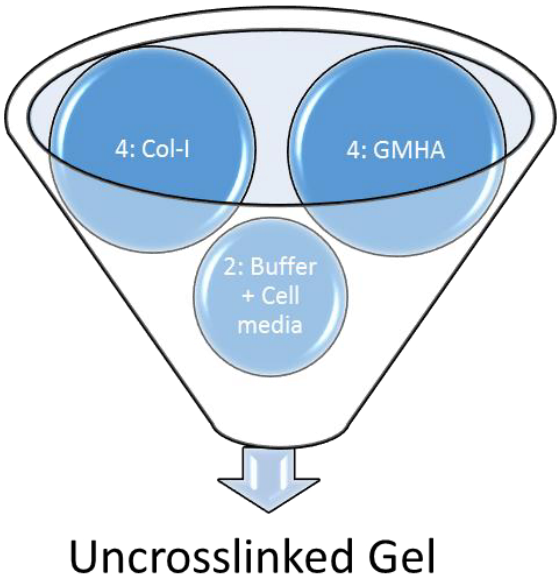

FIGURE 5 MIXING RATIOS

were placed in the middle of each well and each well was then filled with 100 µl cell-free cell medium at 37℃ immediately. The media was added gently to the side of the well so as to not disturb or disrupt the gel. The 96-well plate was placed in a humid incubator at 37℃ with 5% CO2 and incubated overnight in order to allow for the fibrillation of the collagen and cell recovery in case of a matrix containing cells. After the allotted time had passed the gels were crosslinked using 364 nm UV-light for 5 minutes.

2.8 Cell short term survival

Experiments to deduce possible toxicity to the SH-SY5Y cells from UV crosslinking were performed in 2 different ways. First a T25 culture flask containing SH-SY5Y cells were exposed to the same UV-dosage and time required to crosslink the matrix, see Figure 6. This flask was kept for observation and the cell line continued for several passages and subjected to ocular inspection to determine any ill effects. The second method utilized was the inclusion of pure 2D cell controls in all following matrix experiments and observing their viability before and

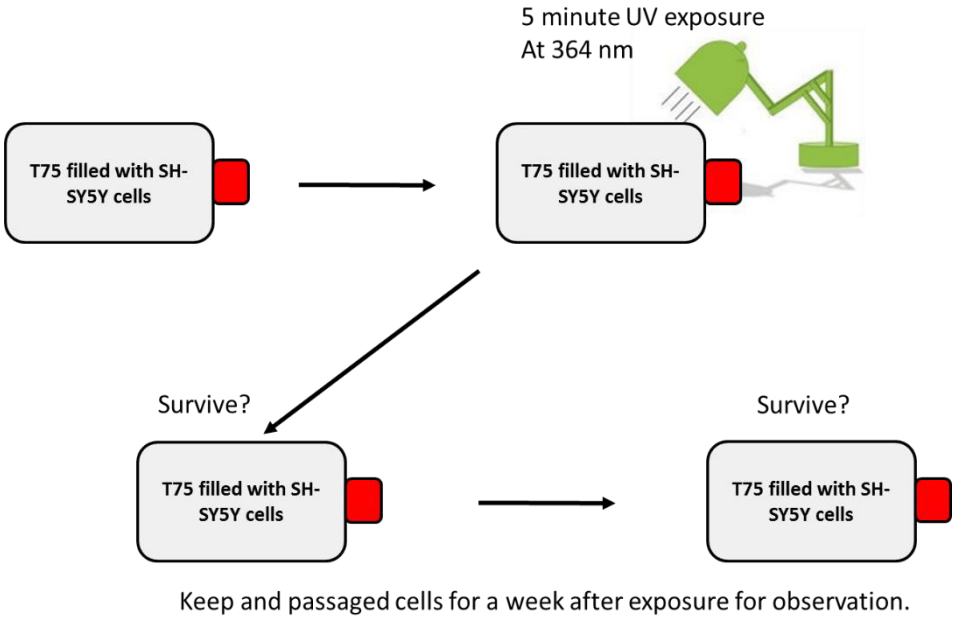

FIGURE 6 FIRST VIABILITY TEST SCHEME.

several time points after UV-crosslinking. The method of assessing viability was comparing the cell morphology with non-UV treated cells and literature, and this method was complemented using Live/Dead-staining.

2.9 Cell long term survival

To determine the viability of the three different cell-types in the matrix a longer term study was performed. 6000 cells/µl gel were seeded in 30 µl gels with four wells for each condition and the gels crosslinked after 12 hours. The media was supplemented with BDNF and the cells were pre-treated for 7 days with RA. The media was changed with fresh media each third day. After 7 days in the matrix cells in the gels were stained using Live/dead staining.

2.10 Cells in 3D

To determine if the cells remained in 3D after seeding several gels were prepared with a cell count of 6000 cells/µl and 30 µl gels as described in 2.9. Incubated for 24 hours before crosslinking and changed media each third day. After 5 days in the matrix the gels were stained using CellTracker (CT).

2.11 Long term comparison model study

The long term comparison model study was performed over 6 weeks in order to allow for the possibility of APP-plaque formation. The study was comprised of 18 conditions split over two main experiments with 9 conditions each that was prepared at the same time, seen in Figure 7.

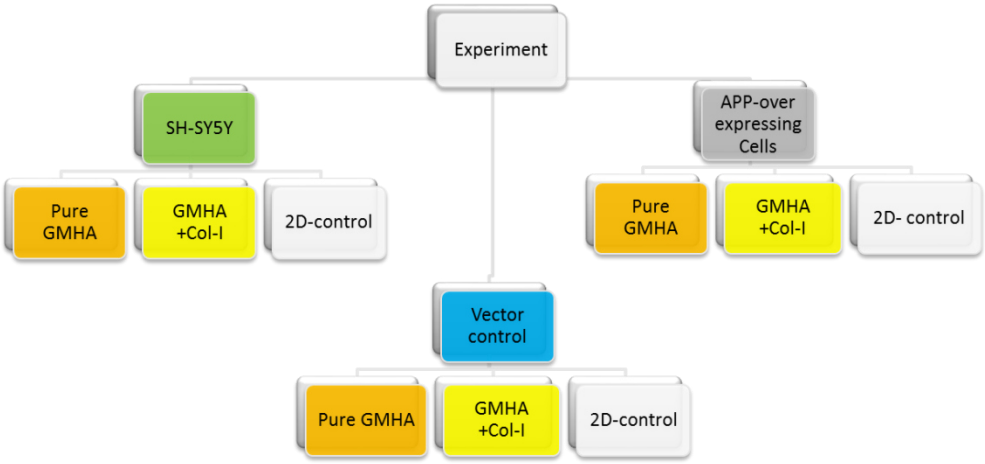

FIGURE 7 CONDITIONS FOR THE 6 WEEK TRIAL.

The cells were pre-differentiated with RA with cell numbers being 180 000 cells per gel and 8000 cells in each 2D control. Each condition was comprised of 4 wells with the same contents. The media was supplemented with BDNF and changed two times per week. Each change, the old media from each single condition were pooled and labelled according to the condition and frozen at -80°C for analysis using electrocytochemistry to determine the presence and ratio of Aβ 38, 40 and 42. At each media change brightfield images were taken in order to perform a morphological comparison between conditions and other models. The only difference between the experiments was the concentration of GMHA in the conditions, 1mg/ml and 2mg/ml respectively. The collagen concentration was kept at 1mg/ml for all conditions containing collagen.

2.12 Electrochemoluminescent Immunosorbent Assay

Electrochemoluminescent Immunosorbent Assay using the Meso Scale Discovery Human (6E10) Abeta Triplex Assay (MDS) as described by the manufacturer (Meso Scale Discovery) was used to screen for the presence of Aβ produced in the matrix during the long-time study. MDS is a protein detection assay that can quantify several different proteins simultaneously in the same sample. The sample is placed in a well where separate predetermined areas have been coated with anti-bodies of Aβx-38/40/42. This assay employs C-terminally specific antibodies to capture the Aβx-38/40/42, respectively, and the 6E10 antibody in combination with a SULFO-TAG-labelled anti-6E10 to quantify the peptides. (*35*). The detection method itself is based on the use of an electric current that triggers the secondary labelled antibody if it is conjugated with the primary antibody, emitting light that can be detected. The light emitted is directly correlated to the amount of the target protein in the sample and as the different antibodies are separated and localised to pre-set positions in the same sample, it is possible to measure the relation between these proteins in a single sample by measuring difference in intensity of the emitted light (*36*).

2.13 Live/Dead staining

The Live/Dead (LD) viability/cytotoxicity kit for mammalian cells(Invitrogen) consists of calcein-AM where the fluorochrome is activated via esterase cleavage once the stain enters a living cell and Ethidium homodimer (EthD), used to detect dead cells. This fluorescent dye cannot penetrate an intact cell membrane as present in

living cells. When EthD enters a cell through a damaged membrane it binds to nucleic acids and the process increases its inherent fluorescence 40-fold, producing a bright red fluorescence.
Practically, the cells were washed two times gently with DMEM x1before staining. Then to 4µM of Calcein-AM and 8µM of EthD were added, the cells were incubated for 20 min at 37C, washed with DMEMx1 and finally fixed with. 8 ℃ cold 4% PFA. The LD images where taken with a confocal laser scanning microscopy system (Leica TCS SP2 RS, Leica Microsystems, Wetzlar, Germany) using HC PL FLUOTAR 20x/0.55 air objective. The dyes are excited at 494 nm for calcein and 528 nm for EthD in succession. The emission light is filtered from the excitation light using bandpass filters, 514/30 nm for Calcein and 609/57 nm for EtHD, all from Semrock. Only green means a healthy cell, while overlap with strong red indicates a dead or dying cell(*37*).

2.14 CellTracker Staining

CellTracker (CT) is a non-toxic fluorescent dye that passes freely through cell membranes and react with the cytosol of the cells into non-permeable fluorescent stable products used in order to track cell movement over time. The dye used, CellTracker Red CMTPX (ThermoFisher) is excited using 2PF 817 nm and detected using a 609/57 (Semroc) filter before the detector (*38*). Before imaging, the cells were prepared in the following way: The cells were washed twice with DMEM x1, 5 µM of celltracker added, incubated for 45min at 37C, washed twice again with DMEM and then fixed with 8 ℃ cold 4% PFA for 10 minutes. To image the cells, the custom non-linear setup was used with a single beam at 817 nm and 30 mW power before the objective, using a Nikon Plan Fluor oil immersion 40×objective with NA 1.3.

2.15 Brightfield Microscopy

Brightfield microscopy with photos was taken through the eyepiece of a Motic AE 2000 microscope using an OptikamB1 Digital Camera, and a Motic 10x/0.25 Ph1 Plan air objective.

2.16 Non-linear microscopy

Images of the samples were acquired using an inverted microscope (Eclipse TE-2000, Nikon). The microscope was fed a laser beam generated from a single picosecond pulsed laser source (Picotrain, HighQ Lasers GmbH).

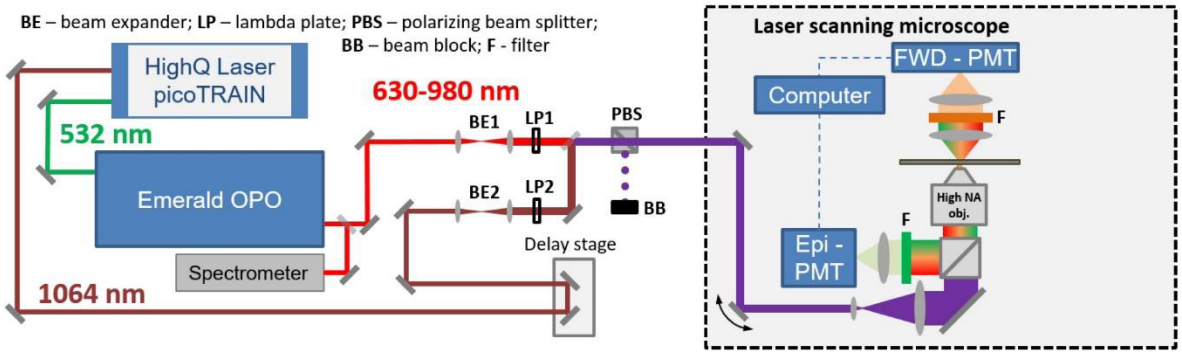

FIGURE 8 SIMPLIFIED MICROSCOPY SETUP PORTRAYING THE OPTICAL LASER PATH OF BOTH PUMP (630-980 NM), AND STOKES 1064 NM BEAMS. ONLY ONE OF THE TWO EPI-DETECTORS ARE SHOWN IN THE SCHEMATIC.

The 532 nm beam was led through an Optical Parametric Oscillator (Emerald OPO, APE GmbH) that allowed for tuning of the wavelength between 630-980 nm. When images are referenced as being taken at 811 nm or 817 nm, it references the wavelength of the laser beam

The microscope, see Figure 8, had three photon detectors consisting of time correlated single photon counting (TCSPC) detectors, one in forward direction (FWD-PMT) and two in epi direction, EPI-side (Epi-PMT) and EPI-back, (not shown) (*39*).

Conventional fluorescence microscopy involves the excitation of a fluorophore with a single photon. This photon excites the fluorophore from the ground state to an electronic excited state. When the excited fluorophore returns to the electronic ground state it results in an emitted photon as seen in Figure 9. The energy difference

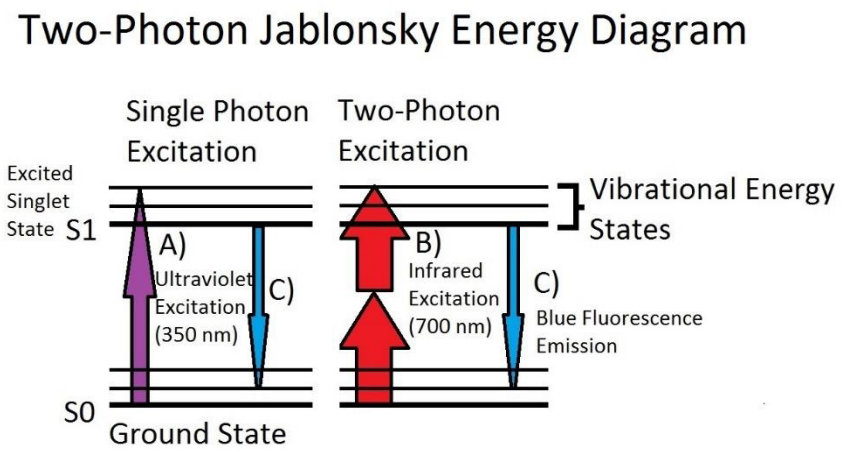

FIGURE 9 DIAGRAM OF A) SINGLE PHOTON EXCITATION AND B) TWO-PHOTON EXCITATION.

between the excitation photon (long straight upwards pointing purple arrow) and the emitted photon (shorter downwards pointing blue arrow) is called the Stokes shift and is caused by non-emitting energy dissipating to the surroundings during the process. The single photon excitation process can be replaced by simultaneous absorption of two or more, higher wavelength photons.

The emitted photon will have the same wavelength in both cases. There are a number of differences and certain advantages of multi-photon microscopy (MPM) over conventional microscopy(*40*). The excitation wavelengths of the photons used in MPM are much longer than the emission wavelength which allows for an easy separation of excitation and emission spectra using different optical filters. Second, the longer wavelength, in the near infra-red regime, allows for a larger penetration depth and lower absorption of photons in the sample and is therefore more suitable for thick biological samples. The requirement of the MPM technique for high peak powers inherently limits the excitation to a small area at the focus. Compared to conventional SPM technique where the beam will excite a much larger area around the focus resulting in called out of focus background fluorescence. The intrinsic confocality of MPM allows for 3D imaging as it is possible to isolate the sample planes with high special resolution and removes the need for a pinhole for this purpose lowering at the same time the induced photo-damage in non-imaging planes. The use of multiple TCSPCs for detection allows for simultaneous excitation and detection of SHG and 2PF(*41*).

2.16.1 Second harmonic generation

Second harmonic generation (SHG) is generated when photons interact with non-centrosymmetric matter. The interaction causes a frequency doubling of the incident wavelength, resulting in the emission of a signal with half the excitation wavelength (being the same as a doubling of the frequency) of the incident photon(*41*). Similarly, to 2PF, the SHG signal is generated only in the tight focus as the process requires high peak power. Collagen fibers are inherently non-centrosymmetric making SHG a widely used technique to image such structures (*42*, *43*). As the molecule is returned to the ground state after the interaction there is theoretically no photo-damage induced.

3. Results and discussion

3.1 Establishing the BME

The important factors to establish before going forward with cells in the BME was collagen distribution, fibrillation and matrix pH. Therefore, several matrices were produced with varying amounts of collagen and HA and the resulting matrices investigated. The effect of incubation times on the matrix was also explored and through an iterative process the BME was prepared for addition of cells.

3.1.1 GMHA preparation

The production of GMHA yielded vastly different amounts of material, 5-20mg output on 50-100mg input. The resulting yield was between 5% at its lowest yield and around 40% at the greatest yield. There are several reasons that could contribute to the consistently low yield of the GMHA. The main factor being that material is poured away along with the supernatant in the precipitation step. Acetone precipitation is documented an inexact process, and it was expected that some material would be lost in the process of decanting(*44*). This could be confirmed by analysing what was poured away in the supernatant seen in Figure 10.

Inspection of the supernatant during the process show spindly structures which indicates that material indeed follows the trimethylamine and Acetone during decanting and is lost. This is not all GMHA aggregates into the desired pellet form in Figure 11, during the centrifuge step. This loss can be countered somewhat by increasing the volume of acetone compared to the GMHA in the falcon tubes as the concentration gradient then shifts more towards the lower part of the tube after centrifuging, and less GMHA should follow the supernatant during decanting.

FIGURE 11 TOP. SUPERNATANT FROM PRECIPITATION, SPINDLY STRUCTURE INDICATED WITH THE RED CIRCLE.

FIGURE 10 RIGHT. GMHA AFTER ONE PRECIPITATION RUN, PELLET MARKED WITH AN ARROW.

Another factor that was identified to impact the available yield is the time the GMHA spends dissolved in the -20 ℃ acetone between centrifugation runs. Longer times than 1 hour facilitates a GMHA that sticks to the tube walls like a coat, seen in Figure 13 compared to Figure 12. This coat will not re-solubilize well in milliQ and is de facto impossible to retrieve using the vacuum freezing method causing further loss of available material.

The zero yield batches occurred due to material fatigue on a bad batch of falcon tubes, as the two batches were

FIGURE 12 GMHA AFTER COMPLETING FREEZE DRYING PROCESS.

FIGURE 13 GMHA LOWER YIELD, AND COAT LIKE RESIDUE SEEN IN FALCON TUBE AFTER LONG TIME IN -20 ℃ ACETONE.

lost when falcon tubes cracked during the centrifuging step and the GMHA turned out to be impossible to salvage.

3.1.2 Collagen addition to GMHA

The effect of adding the Col-I in the GMHA-Col-I matrix was investigated using MPM to answer the following questions, before proceeding to introduce the cell lines into the BME: Can collagen be imaged properly in the GMHA-Col-I gel using MPM, and if we can, how is it distributed? There was also a concern during early imaging that the crosslinker might emit a strong auto-fluorescence that could make cellular studies in the matrix difficult due to overlapping signal spectrums. The crosslinker proved to not affect the MPM imaging.

What was seen, was that the collagen that did form, was spread out in very small fibres that did not form longer strands compared with tissue samples and other in vitro collagen matrices depicted in literature (*45*). The result was unexpected and tracked to inconsistencies the first protocol that resulted in a matrix with a pH that was far too basic to support normal cell or collagen fibre formation.

These results spurred the next study in which the protocol for the matrix creation was adjusted to produce a pH around the physical. This pH study was performed by investigating the respective pH of all components present in the matrix by themselves in order to zero-in on any extremes. During this trial, it was found that it was the combination of the buffer solution and the cell medium that resulted in the aberrant pH. The buffer was adjusted with HCL until pH stabilised around the physical for the finished matrix.

Images of the matrixes formed using the improved protocol was taken in order to answer the previous questions posed, determine any difference in collagen formation, as well as answer the newly proposed question of how the incubation time of the matrix before crosslinking affected the collagen formation. The latter question was brought up as relevant when considering cells in the matrix, and if they would need to recuperate and recover for an extended amount of time between the seeding procedure and the crosslinking, to maximise cell survival rates. The different conditions used in this experiment can be seen in Table 2.

TABLE 2 CONDITIONS FOR COLLAGEN VISUALISATION MATRIX EXPERIMENT

Conditions					
Sample:	**HA control**	**Col-I control**	**GMHA 1.5**	**GMHA 3**	**GMHA 3 24 H**
Col-I mg/ml	0	3	1.5	3	3
GMHA mg/ml	5	0	5	5	5
Incubation time	1 H	1H	1H	1H	24H

The images presented in Figure 14 are of the conditions in Table 2. All images are taken at the same session, with the same imaging settings and at the same depth in the sample. Hence, allowing a direct comparison of the images regarding both homogeneity and intensity.

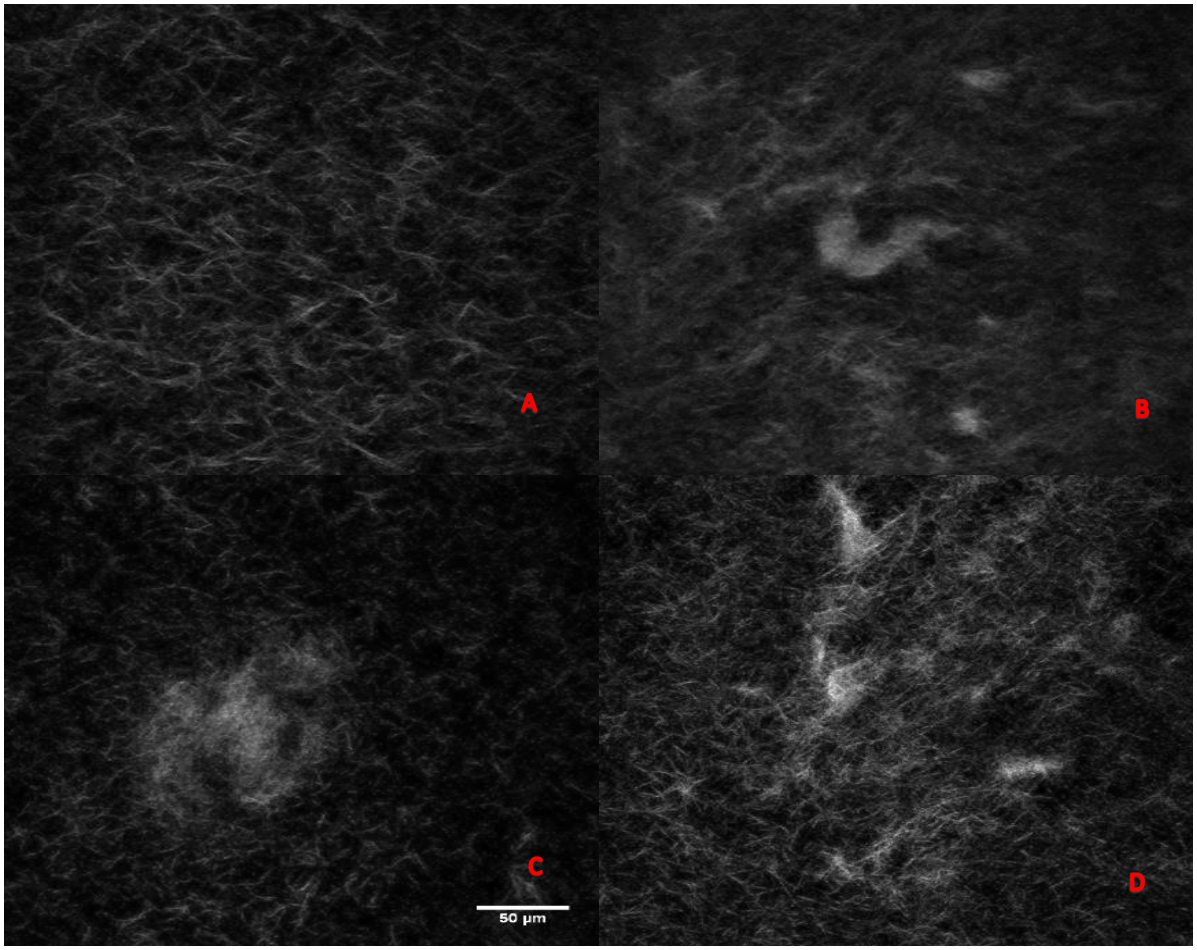

FIGURE 14 COLLAGEN DENSITY AND TIME: PURE COLLAGEN 1.5 MG/ML 1 HOUR INCUBATION (UPPER LEFT) A, GMHACOL-I 3MG/ML 1 HOUR INCUBATION (UPPER RIGHT) B, PURE COLLAGEN 1.5 MG/ML 1 HOUR INCUBATION (LOWER LEFT) C, GMHACOL-I 3MG/ML 24 HOUR INCUBATION (LOWER RIGHT) D. ALL IMAGES ARE REPRESENTABLE LAYERS FROM VOLUME STACKS OF IMAGES (SCALEBAR: 50 µm).

From these images a couple of observations are apparent; 17D contains both brighter features and the same homogenous network seen in the three other conditions. Image 17D is notably brighter over all, an observation that is substantiated by the shift towards brighter features shown in figure 18. The pure Col-I matrix figure 17A, is more homogenous in the both the spread of fibrils and the observed size of the fibrils than the GMHACol-I matrixes seen in figure 17B, 17C and 17D.

This discrepancy between homogeneity is suspected to be because the mixing of the GMHA and Col-I is done by repeated pipetting during a very short time span. The components of the Col-I matrix are in contrast, completely

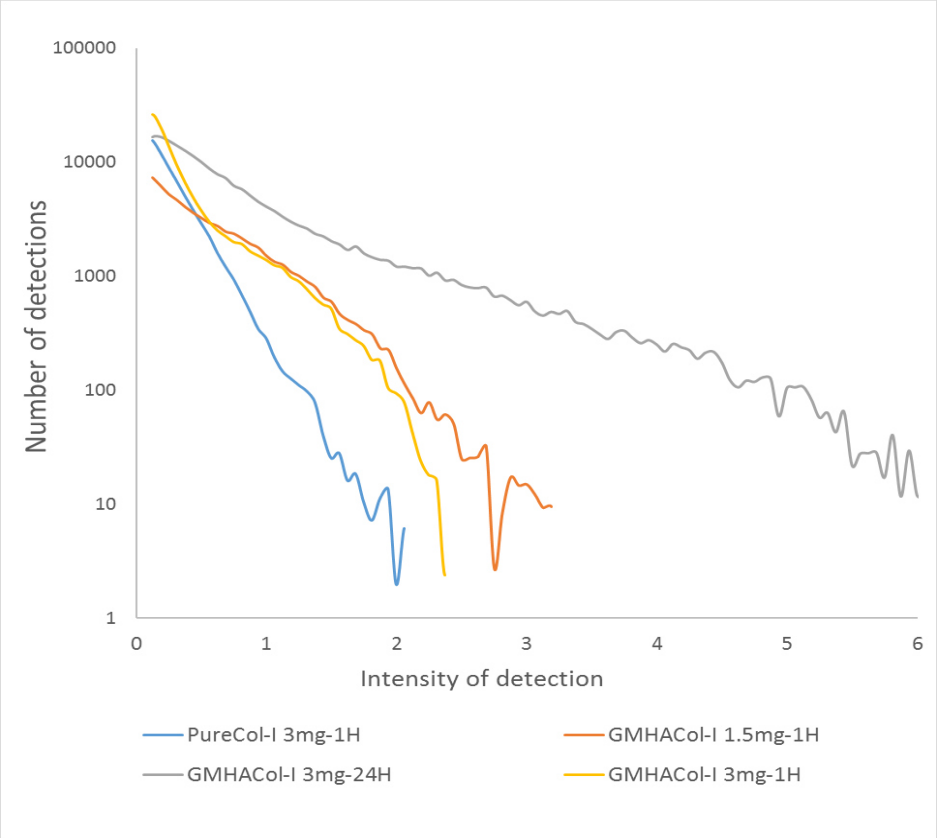

FIGURE 15 LINEARIZED INTENSITY DISTRIBUTION OF COLLAGEN IMAGES IN FIGURE 14. THE GRAPH SHOWS THE TOTAL NUMBER OF DETECTIONS (Y-AXIS), OF DIFFERENT INTENSITY LEVELS (X-AXIS). (THE NUMBER OF PIXELS OF A CERTAIN BRIGHTNESS.)

solubilized in AA and assumed to be a fully homogenous solution from the beginning and that fibrillation therefore should be more even. During later preparations of the matrix the mixing was done more thoroughly as to make sure the cells were present in all parts of the matrix. The distribution of the GMHA itself in the matrixes, is also a factor that could affect the formation of larger Col-I aggregates seen in figure 17B, 17C and 17D and there are dyes that could be used to visualize the HA itself. Characterizing the distribution of GMHA could help in answering why we see these aggregations of Col-I and further studies are recommended. The importance of incubation time is easiest to explore using Figure 15 as the three matrixes with incubation time of 1 hour have similar trends compared to the 24 hour one. As the strength of the SHG signal is quadratic dependent to concentration. Intensity would be related to the size, density and length of the emitting structure, it is reasonable to draw the conclusion that stronger intensity has a relation to larger or longer fibrils being present in the sample. The actual mechanism behind this relation is not investigated; however, it is reasonable to conclude that longer incubation of the matrix facilitates a matrix with a shift towards higher intensity structures, meaning thicker fibers, compared to the other matrixes. According to Roeder *et al.*, polymerisation time is an important factor in 3D-collagen matrix characteristics and adds increased mechanical integrity to the matrix up until around 10 hours of polymerisation, after which it stabilizes(*45*). This adds further credence to the case of the 24-hour incubation being shifted to the right compared to the others in Figure 15 due to the increased amount of high intensity structures.

It was determined that lower concentration of collagen gives a less dense matrix that should allow for an easier imaging once cells are included in the matrix, compare 14B with 14C. The concentration of Col-I does not seem to affect the formation of brighter structures as evident in Figure 15 when comparing the 3 mg/ml 1 hour gel with the 1.5 mg/ml 1 hour gel. However, from the shift towards brighter structures when comparing the 3 mg/ml GMHA 1 hour gel with the 3 mg/ml GMHA 24 hour gel, it appears that the time in incubation before crosslinking

have a large positive impact on fiber size, which is supported in literature(*46*). In conclusion, the decision was made to pursue matrixes with lower Col-I amounts and longer incubation times during the cell trials as it would more closely mimic a brain suffering from head trauma, as the amount of collagen present there is exceedingly sparse and simultaneously allow the cells more time to recuperate.

3.2 Introduction of the cells

Using the result from the BME creation experiments the protocol reached a point where in order to continue with the model, SH-SY5Y cells needed to be introduced and their survival evaluated. First, the undifferentiated cells were used to make fast and rough tuning possible. Then, after the result of the first trials were obtained, the final differentiated cells were evaluated more thoroughly to assess the model.

3.2.1 UV-studies

Experiments to deduce possible toxicity to the SH-SY5Y cells from UV crosslinking was performed as described in the methods chapter.

The result is seen in Figure 16 and the perceived difference in size is due to a lower confluence in the before image, compared to the other two. No immediate noticeable difference was discovered between the cells in the UV-radiated flask when compared to the non-radiated control after the procedure and cells in both flasks showed the same growth rate and morphology. The cells in both UV and Control were kept in culture and passaged twice after exposure and kept for 11 days for observation without any aberrant behaviour observed in either culture. As the unmodified SH-SY5Y were seemingly unaffected by the UV-crosslinking no further test of this nature was performed on the APP-overexpressing line nor on the vector control. It was assumed that the cell-lines would behave in a similar fashion to the unmodified SH-SY5Y when exposed to UV.

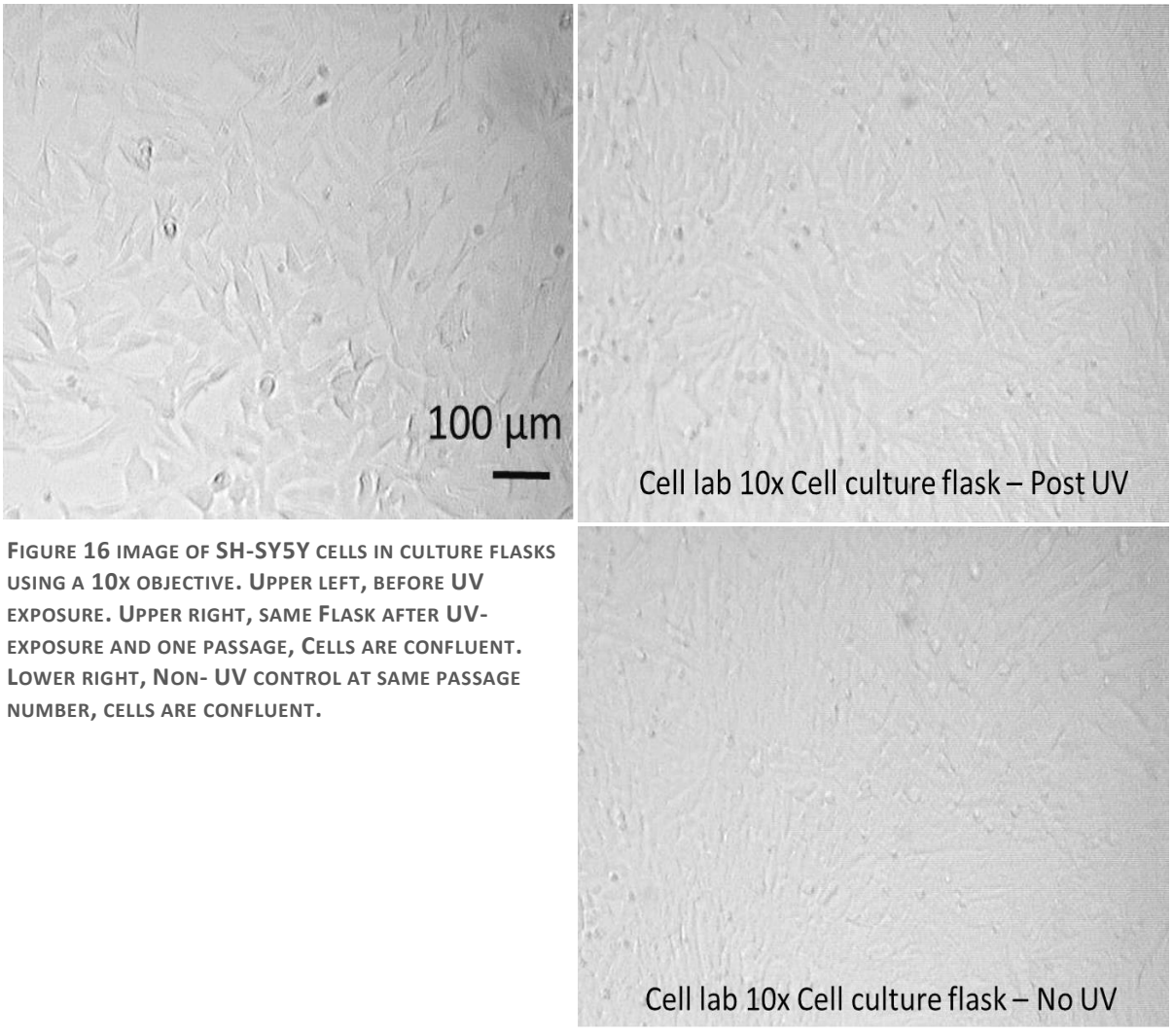

Figure 16 image of SH-SY5Y cells in culture flasks using a 10x objective. Upper left, before UV exposure. Upper right, same Flask after UV-exposure and one passage, Cells are confluent. Lower right, Non- UV control at same passage number, cells are confluent.

3.2.3 Cells in 3D

In order to establish if the cells would keep being suspended in 3D within the BME, or slowly sink to the bottom of the 96-wellplates. An experiment was performed where SH-SY5Y cells were RA-differentiated for 7 days in culture and then densely seeded, 8000 cells/µl in 30 µl gels, in a GMHA-matrix with a collagen concentration of 1 mg/ml. The gel was crosslinked the day after seeding, after at least 10 hours of incubation. The cells were cultured in the gels for 5 days before imaging. The images shown in Figure 17 are different angles of a 3D rendered view of a stack of individual planes, or slices. Each slice making up the image is taken with a spacing of 1.5 µm above the previous slice, starting at the oil/glass boundary underneath the well plate. The image has been treated in imageJ by thresholding to show the strongest signal in order to only show the central cell bodies, as the neurites obscured the view. As seen in Figure 17, the cells are suspended above the bottom of the well. However, some cells seem to grow directly on top of the glass which is confirmed using z-stacks (not shown).

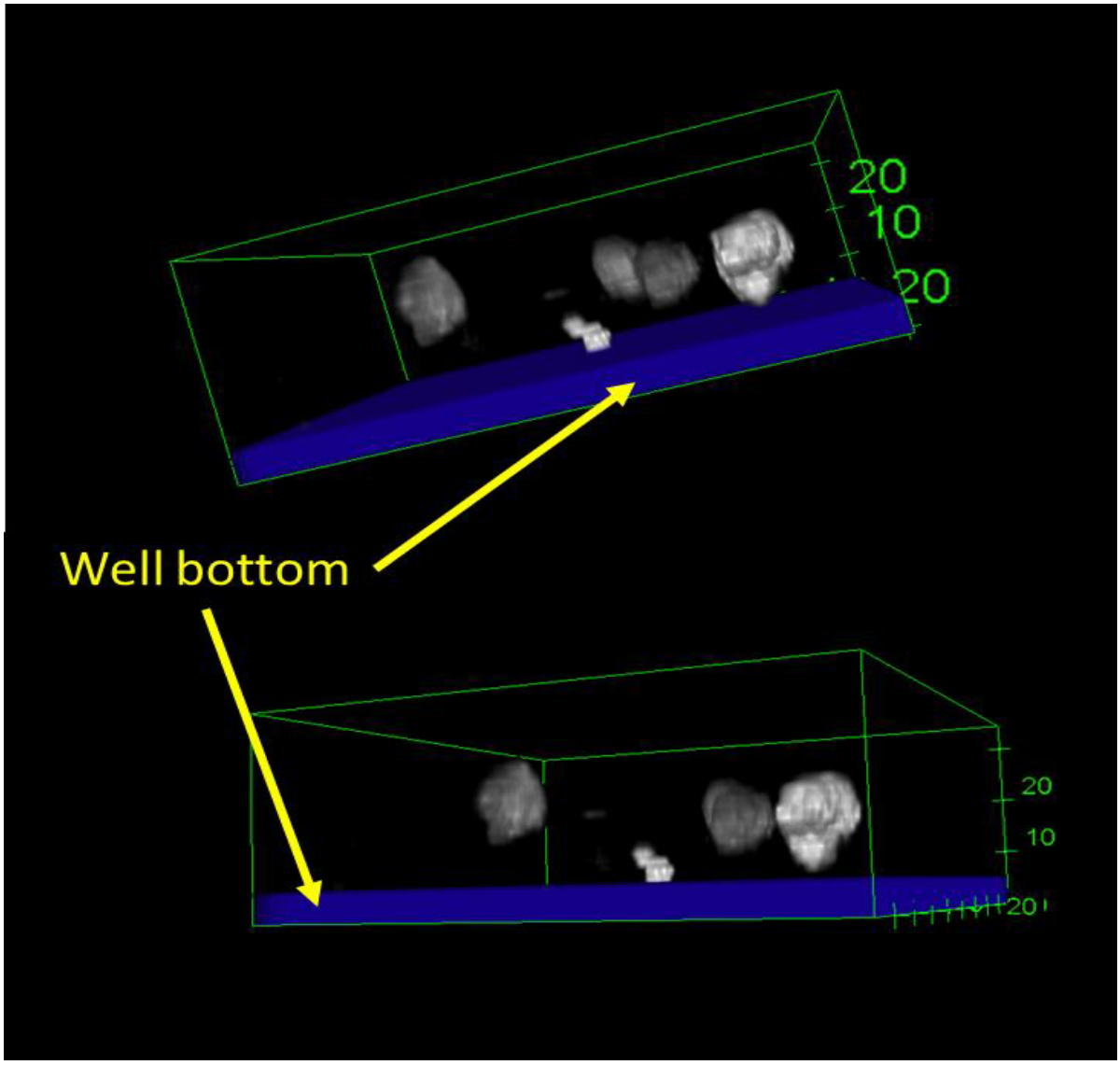

FIGURE 17 3D RENDERING OF Z-STACK USING CELLTRACKER TO TRACE CELL-BODIES 5 DAYS AFTER SEEDING IN MATRIX.

3.2.4 Live/Dead

The LD studies where performed on RA-differentiated cells that spent 8 days in the matrix before the assay. Images were taken at different depths in the sample showing cells at different heights within the matrix as well as the direct surface of the glass, as seen in Figure 18. Both bigger rounded cells as well as more neuron-like cells showing ganglia like outgrowth show as green and healthy. There are also some co-localization of green and red dyes showing up as yellow, meaning cells are either unable to keep their membranes intact or cell debris from dead cells are accumulated around them. The morphology of these dying cells are typically small, shrivelled rounded and grain like, while the larger cells and the cells showing protrusions show up as healthy. Comparison with LD studies by Imamura *et al.*, who used RA-differentiated cells in 3D-environments in Parkinson studies, show a similar morphology for the live cells as well as the same shrunken grain like pattern for the dead cells (*47*). This morphological information is used as a base to argue the vitality of the cells during the 6-week trial as LD staining during the 6-week long trial would make it necessary to sacrifice the investigated wells each time.

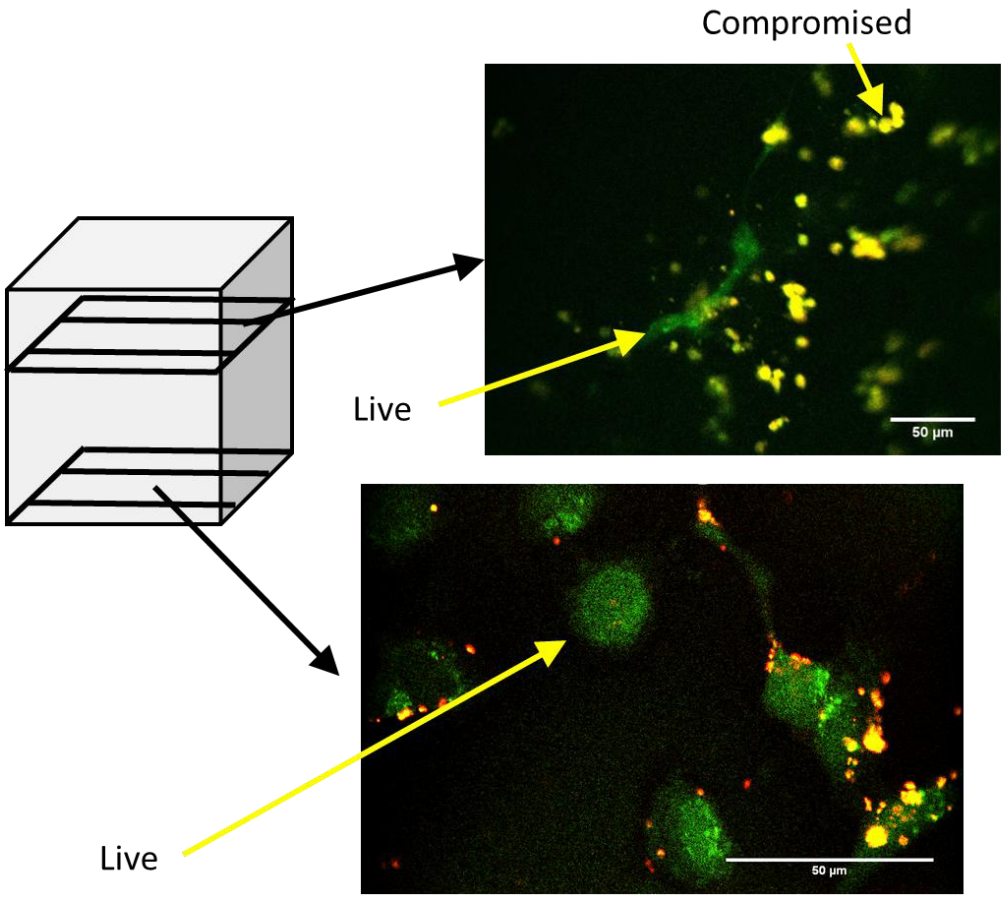

FIGURE 18 LIVE/DEAD STAINING OF SH-SY5Y CELLS AT DIFFERENT HEIGHTS IN THE MATRIX. IMAGES TAKEN OF RA-DIFFERENTIATED CELLS AFTER 8 DAYS IN THE MATRIX.

3.3 Long term Brightfield study

The 6-week trial was based on two cornerstones, morphology and excreted factors in the media. Using these in tandem, conclusions about the model can be drawn. From both the LD-study and previously described as well as other 3D-studies using SH-SY5Y cells (*47*) it is shown that the morphology of the cell can be tied to the health of said cell. Images where taken at every media change before removing media for freezing. The images of each condition were then analysed and scored according to morphology, confluency and neurite length. The scores are presented in table 3. Criterions are valid for the majority of cells and across multiple repeats of each conditions. The criterions followed this system:

Morphology: Stretched, Stretched cells or cells with non-round morphology. Mixed, no clear majority of any morphological type. Grain, small round cells.

Confluency: Confluent, cells covers more than approximately 70% of the image area. Interconnected, cells cover less than 70 % of the image area but there is a high presence of interconnected cells or clustering of cells. Sparse cells, single cells or no cells.

Neurite length: Long, neurite longer than 3 times the cell body. Short, thin short extension from cell body.

Week 0, at the 3-day mark, all conditions behaved similarly. Confluent and stretched with the notable exception

TABLE 3 6-WEEK BRIGHTFIELD STUDY.

Cell	Condition	Week 0			Week 1			Week 2			Week 3			Week 4			Week 5			Week 6		
		M	C	NL	M	C	NL	M	C	NL	M	C	NL	M	C	NL	M	C	NL	M	C	NL
SH-SY5Y	2D-control	++	+	0	+	+	+	0	0	0	0	0	0	0	0	0	0	0	0	0	0	0
Vector control	2D-control	++	+	0	+	+	0	0	0	0	0	0	0	0	0	0	0	0	0	0	0	0
APP	2D-control	++	+	0	+	+	+	0	0	0	0	0	0	0	0	0	0	0	0	0	0	0
SH-SY5Y	GMHA 1 mg/ml	++	++	0	++	++	+	++	++	+	0	+	0	0	0	0	0	0	0	0	0	0
Vector control	GMHA 1 mg/ml	++	++	0	+	++	0	+	+	0	0	0	0	0	0	0	0	0	0	0	0	0
APP	GMHA 1 mg/ml	++	++	0	++	++	0	++	+	+	+	+	++	+	+	++	0	0	0	0	0	0
SH-SY5Y	GMHA 1 mg/ml +Col-I	++	++	0	++	++	0	++	+	++	0	+	++	0	0	0	0	0	0	0	0	0
Vector control	GMHA 1 mg/ml + Col-I	++	++	0	+	++	0	+	0	0	0	0	0	0	0	0	0	0	0	0	0	0
APP	GMHA 1 mg/ml + Col-I	++	++	0	+	++	0	+	+	+	0	+	+	0	0	0	0	0	0	0	0	0
SH-SY5Y	GMHA 2 mg/ml	++	++	0	+	++	0	++	++	0	++	++	0	+	+	++	0	0	0	0	0	0
Vector control	GMHA 2 mg/ml	++	++	0	++	++	0	+	+	0	0	+	0	0	+	0	0	+	0	0	+	0
APP	GMHA 2 mg/ml	+	++	0	+	+	+	+	+	0	0	+	0	+	+	0	0	+	0	0	+	0
SH-SY5Y	GMHA 2 mg/ml + Col-I	++	++	0	++	+	+	++	+	+	+	+	++	++	+	++	+	+	++	0	0	0
Vector control	GMHA 2 mg/ml + Col-I	++	++	0	+	+	0	+	+	0	0	+	0	0	+	0	0	0	0	0	0	0
APP	GMHA 2 mg/ml + Col-I	+	++	0	+	+	0	+	+	0	0	0	0	0	0	0	0	0	0	0	0	0
M = Morphology of cells:		++ Stretched		+ Mix	0 Grain-like			C = Confluency:		++ Confluent	+ Interconnected			+ Sparse cells			NL = Neurite length:		++ Long	+ Short		0 None

of both of the 2 mg/ml APP conditions, that are not confluent. The reason for the disparity in the APP conditions might be found in less cell numbers than expected in the seeding phase, as both conditions in the 2 mg/ml show the same trend and are from the same seeding. Thus, a comparison of the 1 and 2 mg/mg APP needs to take into account the difference in starting number of cells between the conditions.

This could also skew the results from the Electrochemoluminescent Immunosorbent Assay, Figure 19, performed on the media from these conditions. The vector control conditions unexpectedly do not behave the same way as the SH-SY5Y conditions. Almost all conditions have had their cell numbers being completely deteriorated by week 3 and the 21 day mark, with the exception of APP 1mg/ml GMHA, APP 2mg/ml GMHA, SH-SY5Y 2 mg/ml GMHA and SH-SY5Y 2mg/ml GMHA +Col-I. This indicates that increased HA density have a positive effect on the cells and by comparing Figure 19 condition by condition with Figure 20 the 2 mg/ml conditions show longer neurites as well as more extensive branching. The collagen containing conditions showed reduced confluency

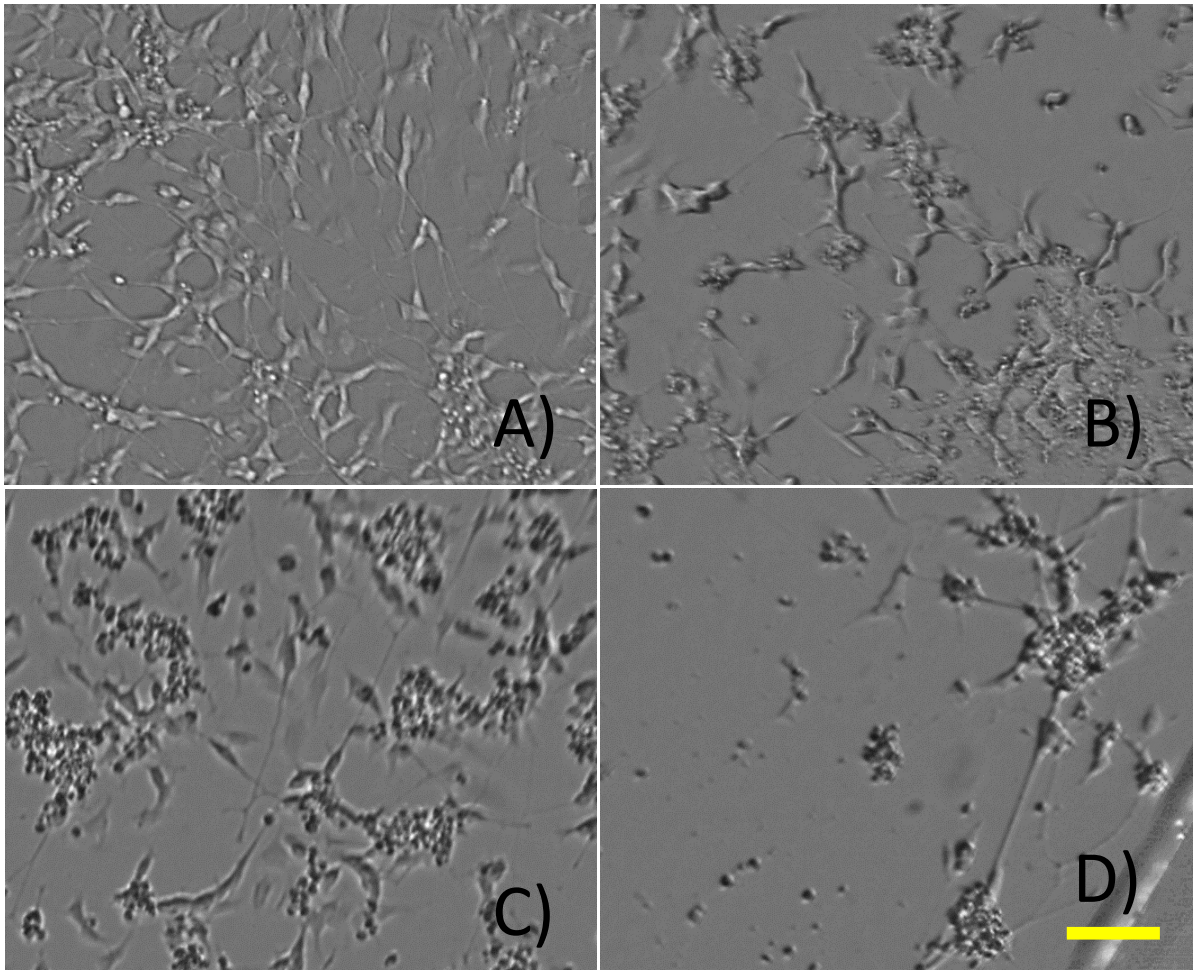

FIGURE 19A) SH-SY5Y GMHA 1MG/ML 13 DAYS B) SH-SY5Y GMHA + COL-1 1MG/ML 13 DAYS C) APP-OVEREXPRESSING GMHA 1 MG/ML 13 DAYS D) APP-OVEREXPRESSING GMHA + COL-I 1 MG/ML 13 DAYS. IMAGES TAKEN WHEN NEURITES WHERE FIRST SPOTTED IN EACH CONDITION BUT DUE TO DIFFERENT LEVELS OF CONFLUENCY OBSTRUCTING THE VIEW THE TIME POINTS VARY A LOT. SCALE BAR 100 µM

compared to the pure GMHA conditions for both APP and vector control conditions. SH-SHY5 however, had a positive reaction to the collagen presence showing both increased confluency, lasting longer in the matrix and increased neurite length across both the 1 mg/ml and 2 mg/ml conditions. The difference in how long before the cells deteriorate in the matrix is interesting, as according to literature differentiated SH-SY5Y cells are known to be stable for up to 21 days in vitro(*48*) in perfusion culture, and 14 days with a pure RA differentiation protocol in 2D (*49*). The caveat however is that the cells used in both of those studies had a much lower passage number compared to the ones used in this matrix study. Furthermore there are also long term studies showing the possibilities of growing the SH-SY5Y cells for extended periods after neuronal differentiation, as shown by Constantinescu *et al.* in 2007 (*50*) showing healthy cells 2 months after differentiation by using additional supplements. Comparing the morphology of the cells in the 6 week trial with those presented by Agholme et al. for the first 3 weeks show remarkable similarities in neurite morphology (*27*), figure 24 a and b.

The conditions with a higher concentration of HA during the morphological study had a more stable morphology and less rapid deterioration as seen in Table 3. The media from the high HA concentration was thus chosen for the APP triplex assay study with the reasoning that more cells would grant a more stable reading on excreted

proteins. Changing all media at once each time might have had a negative impact as SH-SY5Y cells have been reported to be sensitive to sudden changes in the environment (*48*).

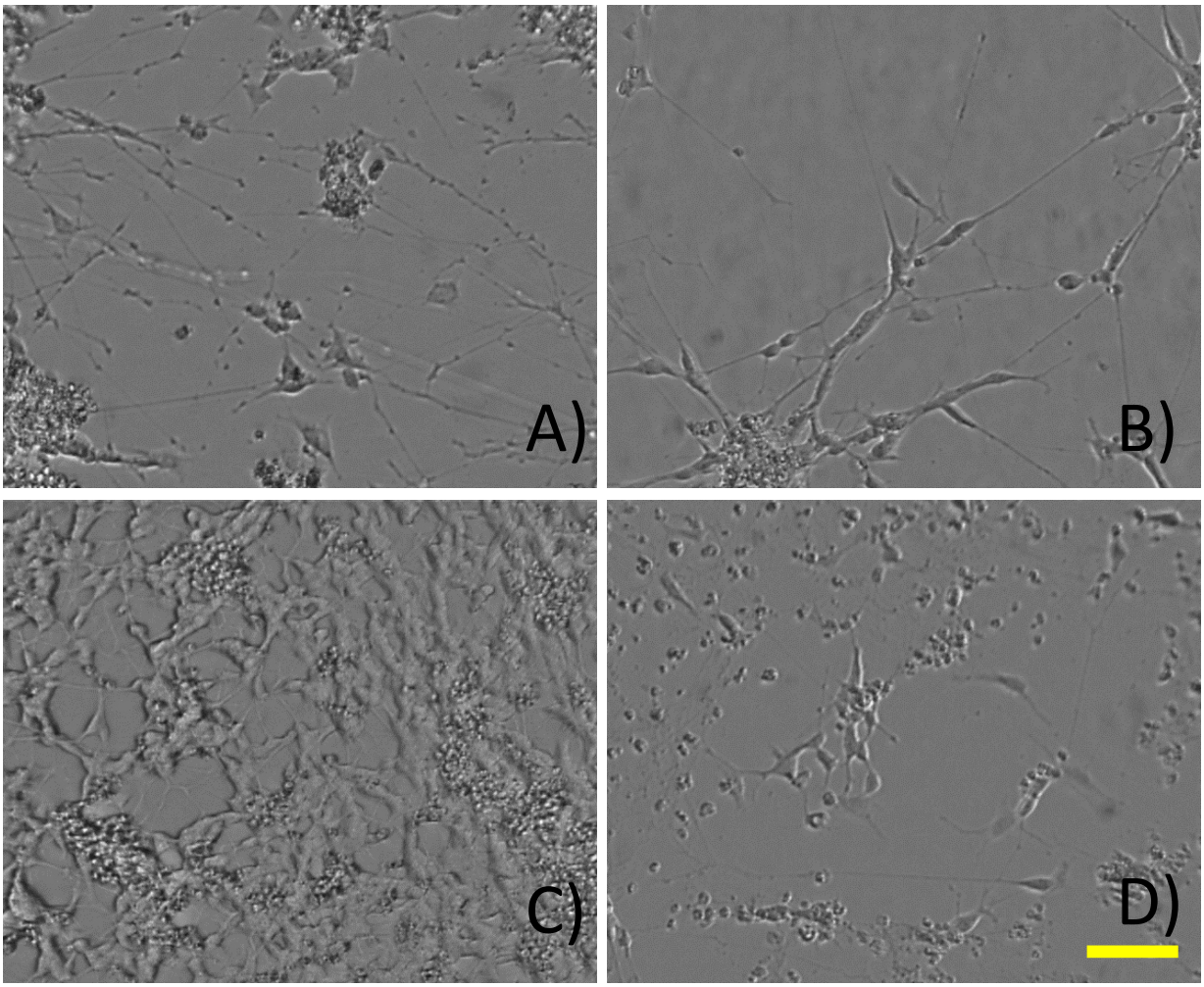

FIGURE 20 A) SH-SY5Y GMHA 2 MG/ML 31 DAYS B) SH-SY5Y GMHA + COL-1 2 MG/ML 17 DAYS C) APP-OVEREXPRESSING GMHA 2 MG/ML 10 DAYS D) APP-OVEREXPRESSING GMHA + COL-I 2 MG/ML 10 DAYS. IMAGES TAKEN WHEN NEURITES WHERE FIRST SPOTTED IN EACH CONDITION BUT DUE TO DIFFERENT LEVELS OF CONFLUENCY OBSTRUCTING THE VIEW THE TIME POINTS VARY A LOT. SCALE BAR 100 µM

3.3.1 Electrochemoluminescent Immunosorbent Assay

The results of the brightfield study indicated that the most promising conditions were containing high concentration of Hyaluronic acid. The 2 mg/ml conditions lasted longer in the trial and thus only the media from the 9 conditions of 2mg/ml GMHA and the 2 mg/ml GMHA + Col-I were analysed for the expression of Aβ 38, 40 and 42 after the 6-week trial was completed. The study utilized the saved frozen media samples taken 2 times each week for the 6 weeks. One sample per condition and week was used starting with day 3 at the first media change. The data from Aβ 38, as well as all data from the 2D controls are omitted as levels were below detection threshold. Data from week 6 is also below threshold for all conditions as well and therefore omitted. The detection thresholds are 36.4 pg/ml for Aβ 40 and 0.94 pg/ml for Aβ 42. Differing total number of cells as the trial progressed may have affected the amounts of excreted factors detected in the media. Comparison between

the different conditions are still possible however as the pooling of media across the entire condition allows collection of a higher total of excreted factors at the cost of specificity in regards to individual well-morphology.

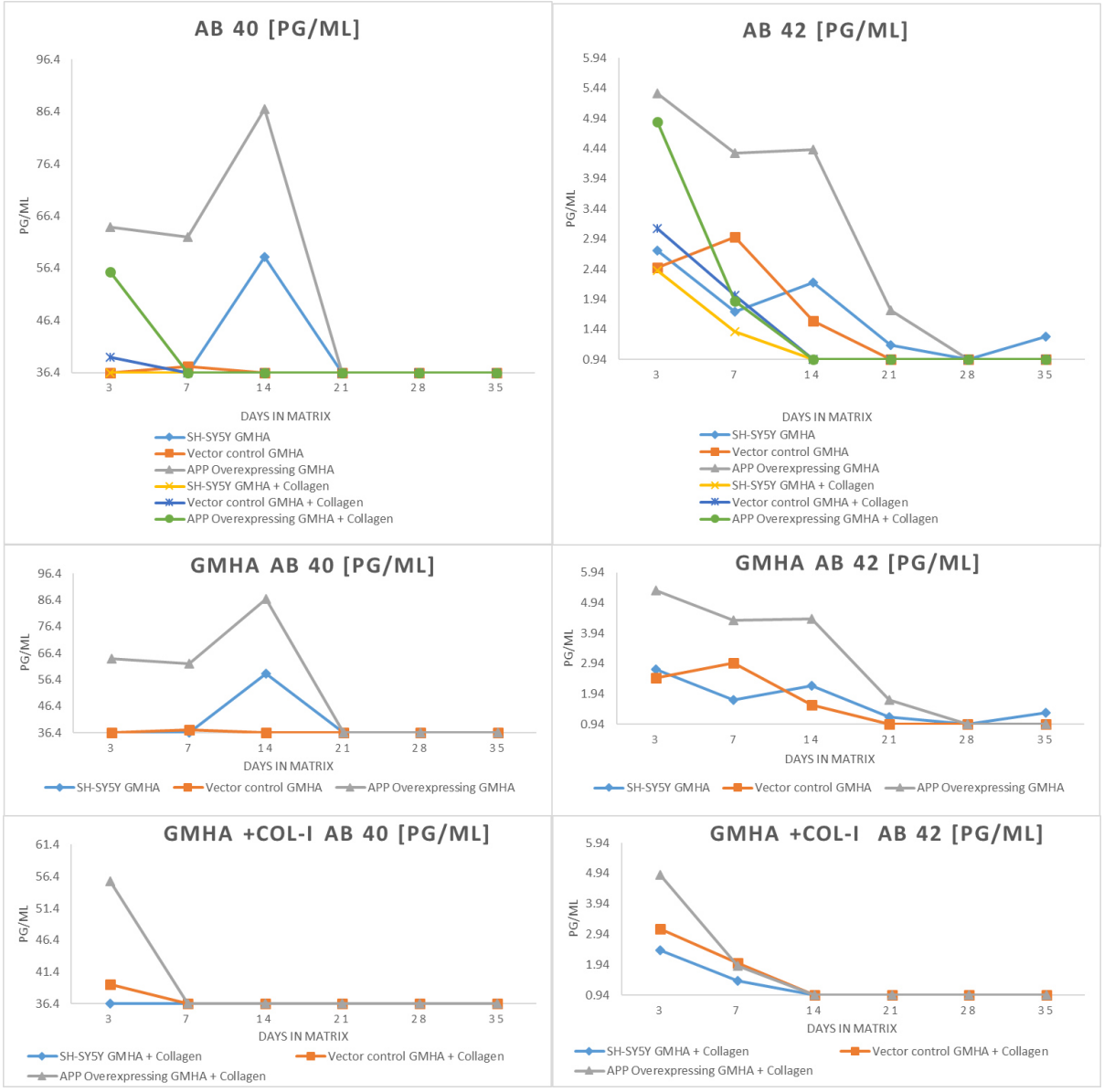

FIGURE 21 RESULT OF MDS TRIPLEX ASSAY MEDIA ANALYSIS OF THE 2 MG/ML CONDITIONS OF THE 6 WEEK TRIAL. TOP GRAPHS SHOW ALL CONDITIONS BUNDLED TOGETHER FOR AN OVERVIEW WHILE THE MIDDLE AND BOTTOM ONES SHOW PURE GMHA AND GMHA + COL-I RESPECTIVELY.

Some interesting trends appear when analysing the graphs in Figure 21. First, the difference between pure GMHA and Col-I conditions, in that the Col-I containing conditions show a decreasing curve across all conditions while the pure GMHA conditions both varies more over time. Then, the fact that the Vector control once again show a different behaviour compared to both the APP and the SH-SY5Y conditions indicates further studied including a more thorough characterisation and validation of the cells are needed.

The graphs show a peak occurring around day 14 in both SH-SY5Y and APP GMHA conditions for Aβ 40 which is unfortunately not possible to connect with any unique morphology such as neurite length as both conditions are confluent during this time. A similar pattern is seen in Aβ 42. Surprisingly and interestingly enough Aβ 42 goes down only to resume being secreted in detectable levels all the way up to day 35 even though not a lot of cells remain at that point. One explanation could be that the cells react negatively to having the entire media with excreted factors being removed and forcing a hard reset of cell condition every media change. Some

protocols suggest changing only half the media at each point as to not disturb the cells to much which could also potentially explain the rapid deterioration of some of the conditions(*48*).

Interestingly when comparing Figure 21 with Table 3 the Col-I conditions exhibit less cells, earlier confluency loss and show a rapid decline in Aβ in the media, compared to the pure GMHA conditions. One could speculate that the Aβ and the collagen interacts in some way as to reduce the amount of free Aβ in the media.

4. Conclusion

The matrix characteristics are tuneable and different concentrations of GMHA and GMHA+Col-I elicited a different response in the cellular behaviour. The cells are in 3D; however, the nature of the study make it hard to interpret if it was the 3D itself or the differing GMHA concentrations that made the cells prefer the matrix compared to the 2D control and that needs to be addressed in further work. The model shows some promise for use in differentiating SH-SY5Y to neuron-like morphologies and especially the fact that the materials and factors involved is well defined is useful for studies of ECM components impact on the neuronal function and comparison studies with previously established models using Matrigel. The most promising conditions in the matrix show neuron-like cells that exhibit comparable morphology to those presented by Agholme *et al.*(*27*) and other previous differentiation studies on SH-SY5Y(*34*, *48–50*). However, the conflicting behaviour of the vector control and both SH-SY5Y and the APP overexpressing variant suggest that further refinement of the matrix protocol is still needed before it can be used as a reliable neuronal model. The APP study suggest that ECM components could play a part in either expression too or the free movement of APP in the surrounding brain, resulting in neuronal dysfunction but further studies are necessary before the model could be used reliably in AD research.

5. Further work

To further validate the model the experiment should be repeated at least two more times. Instead of the pure glass control, GMHA and GMHA+Col-I coated 2D-controls should be introduced for each condition to discern if the 3D-matrix is necessary, or even just supplement the medium with the ECM components in ordinary culture conditions to discern if it is merely the presence of ECM material that matters. It would also be interesting to further optimise the conditions after seeding the cells in the matrix with different neuronal maintenance media for instance, and see if that could stabilize the conditions past 21 days after the long neurites appear. Studies should be performed with SH-SY5Y cells, APP and Vector control that are at an initial lower passage number in order to reduce the risk of aberrant behaviour.

Further characteristics of the cells, such as performing staining for neuronal markers such as Tau etc. that are affiliated to functional neurons in order to substantiate the claims that the cells are in fact behaving like neurons would be critical. Studies on possible electrical synapse activity could also be performed by for instance Ca+ imaging or a patch clamp assay.

For studies performed in the model itself, ECM remodelling studies would be very interesting to pursue as well as different versions of co-culturing with for instance astrocytes or neuroglia cells as they are involved with brain ECM and neuronal health.

References

1. W. H. O. Mental, H. Gap, A. Programme, Media centre Dementia, 6–9 (2012).
2. B. L. Plassman *et al.*, Documented head injury in early adulthood and risk of Alzheimer's disease and other dementias. *Neurology*. **55**, 1158–1166 (2000).
3. W. B. Zigman *et al.*, Alzheimer's Disease in Adults with Down Syndrome. *Int. Rev. Res. Ment. Retard.* **36**, 103–145 (2008).
4. M. E. Weksler *et al.*, Alzheimer's disease and Down's syndrome: Treating two paths to dementia. *Autoimmun. Rev.* **12**, 670–673 (2013).
5. S. H. Choi *et al.*, A three-dimensional human neural cell culture model of Alzheimer's disease. *Nature*. **515**, 274–8 (2014).
6. G. Raivich *et al.*, Molecular signals for glial activation: pro- and anti-inflammatory cytokines in the injured brain. *Acta Neurochir Suppl*. **73**, 21–30 (1999).
7. P. Grammas, A damaged microcirculation contributes to neuronal cell death in Alzheimer's disease. *Neurobiol. Aging*. **21**, 199–205 (2000).
8. J. M. Nussbaum, M. E. Seward, G. S. Bloom, Alzheimer disease: a tale of two prions. *Prion*. **7**, 14–19 (2013).
9. E. Mohandas, V. Rajmohan, B. Raghunath, Neurobiology of Alzheimer's disease. *Indian J. Psychiatry*. **51** (2009), pp. 55–61.
10. V. W. Chow, M. P. Mattson, P. C. Wong, M. Gleichmann, An overview of APP processing enzymes and products. *Neuromolecular Med.* **12**, 1–12 (2010).
11. H. Zheng, E. H. Koo, Molecular Neurodegeneration The amyloid precursor protein: beyond amyloid. *Mol. Neurodegener.* **1**, 1–12 (2006).
12. A. L. Phinney *et al.*, No hippocampal neuron or synaptic bouton loss in learning-impaired aged ??-amyloid precursor protein-null mice. *Neuroscience*. **90**, 1207–1216 (1999).
13. Alzheimer's Society, What is Alzheimer's disease ? *Factsheet 401LP*. **2**, 1–11 (2014).
14. C. Ballard *et al.*, Alzheimer's disease. *Lancet*. **377**, 1019–1031 (2011).
15. J. Wegiel *et al.*, Intraneuronal Aβ immunoreactivity is not a predictor of brain amyloidosis-β or neurofibrillary degeneration. *Acta Neuropathol.* **113**, 389–402 (2007).
16. M. S. Cheon, M. Dierssen, S. H. Kim, G. Lubec, Protein expression of BACE1, BACE2 and APP in Down syndrome brains. *Amino Acids*. **35**, 339–343 (2008).
17. E. Karousou *et al.*, New insights into the pathobiology of Down syndrome--hyaluronan synthase-2 overexpression is regulated by collagen VI alpha2 chain. *FEBS J.* **280**, 2418–2430 (2013).
18. E. Ruoslahti, Brain extracellular matrix. *Glycobiology*. **6**, 489–492 (1996).
19. J. B. Leverenz, M. A. Raskind, Early Amyloid Deposition in the Medial Temporal Lobe of Young Down Syndrome Patients: A Regional Quantitative Analysis. *Exp. Neurol.* **150**, 296–304 (1998).

20. H. M. Wisniewski, J. Wegiel, The neuropathology of Alzheimer's disease. *Neuroimaging Clin. N. Am.* **5**, 45–57 (1995).

21. E. Head, D. Powell, B. T. Gold, F. A. Schmitt, Alzheimer's Disease in Down Syndrome. *Eur. J. Neurodegener. Dis.* **1**, 353–364 (2012).

22. E. Kida, K. E. Wisniewski, H. M. Wisniewski, Early amyloid -β deposits show different immunoreactivity to the amino- and carboxy-terminal regions of β-peptide in Alzheimer's disease and Down's syndrome brain. *Neurosci. Lett.* **193**, 105–108 (1995).

23. V. E. Johnson, W. Stewart, D. H. Smith, Traumatic brain injury and amyloid-β pathology: a link to Alzheimer's disease? *Nat. Rev. Neurosci.* **11**, 361–70 (2010).

24. S. Gottlieb, Head injury doubles the risk of Alzheimer's disease. *Br. Med. J.* **333**, 7575 (2006).

25. C. Van den Heuvel *et al.*, Upregulation of amyloid precursor protein messenger RNA in response to traumatic brain injury: an ovine head impact model. *Exp. Neurol.* **159**, 441–450 (1999).

26. T. Hashimoto *et al.*, CLAC: A novel Alzheimer amyloid plaque component derived from a transmembrane precursor, CLAC-P/collagen type XXV. *EMBO J.* **21**, 1524–1534 (2002).

27. L. Agholme, T. Lindström, K. Kgedal, J. Marcusson, M. Hallbeck, An in vitro model for neuroscience: Differentiation of SH-SY5Y cells into cells with morphological and biochemical characteristics of mature neurons. *J. Alzheimer's Dis.* **20**, 1069–1082 (2010).

28. S. Suri, C. E. Schmidt, Cell-laden hydrogel constructs of hyaluronic acid, collagen, and laminin for neural tissue engineering. *Tissue Eng. Part A*. **16**, 1703–1716 (2010).

29. Y. H. Kim *et al.*, A 3D human neural cell culture system for modeling Alzheimer's disease. *Nat. Protoc.* **10**, 985–1006 (2015).

30. C. S. Hughes, L. M. Postovit, G. A. Lajoie, Matrigel: a complex protein mixture required for optimal growth of cell culture. *Proteomics*. **10**, 1886–1890 (2010).

31. J. R. Harris, A. Soliakov, R. J. Lewis, In vitro fibrillogenesis of collagen type I in varying ionic and pH conditions. *Micron*. **49**, 60–68 (2013).

32. J. L. Biedler, S. Roffler-Tarlov, M. Schachner, L. S. Freedman, Multiple neurotransmitter synthesis by human neuroblastoma cell lines and clones. *Cancer Res.* **38**, 3751–7 (1978).

33. J. L. Biedler, L. Helson, B. A. Spengler, Morphology and Growth, Tumorigenicity, and Cytogenetics of Human Neuroblastoma Cells in Continuous Culture. *Cancer Res.* **33**, 2643–2652 (1973).

34. H. Xie, L. Hu, G. Li, SH-SY5Y human neuroblastoma cell line: in vitro cell model of dopaminergic neurons in Parkinson's disease. *Chin. Med. J. (Engl).* **123**, 1086–1092 (2010).

35. V. Plus, M. Kits, S. Kits, AB Peptide Panel 1 Kits, 1–29.

36. J. R. Forster, P. Bertoncello, Keyes E. Tia, Electrogenerated Chemiluminescence. *Annu. Rev. Anal. Chem.* **2**, 359–85 (2009).

37. Invitrogen Molecular Probes, LIVE/DEAD Viability/Cytotoxicity Kit for mammalian cells. *Prod. Information, Cat. number MP 03224*, 1–7 (2005).

38. T. F. S. Inc, CellTracker ™ Fluorescent Probes, pp. 1–5.

39. A. Enejder, C. Brackmann, F. Svedberg, Coherent Anti-Stokes Raman Scattering Microscopy of Cellular Lipid Storage. *IEEE J. Sel. Top. Quantum Electron.* **16**, 506–515 (2010).

40. D. Piston, T. Fellers, Fundamentals and applications in multiphoton excitation microscopy. *Nikon*. **c**, 9 (2012).

41. A. Krueger, Multiphoton microscopy : Turnkey femtosecond lasers fuel growth of multiphoton imaging. *LaserFocusWorld*. **46**, 1–7 (2010).

42. G. Cox, E. Kable, Second-harmonic imaging of collagen. *Methods Mol. Biol.* **319**, 15–35 (2006).

43. X. Chen, O. Nadiarynkh, S. Plotnikov, P. J. Campagnola, Second harmonic generation microscopy for quantitative analysis of collagen fibrillar structure. *Nat Protoc*. **7**, 654–669 (2012).

44. Pierce, Acetone precipitation of proteins. **747**, 7–8 (2007).

45. B. A. Roeder, K. Kokini, J. E. Sturgis, J. P. Robinson, S. L. Voytik-Harbin, Tensile Mechanical Properties of Three-Dimensional Type I Collagen Extracellular Matrices With Varied Microstructure. *J. Biomech. Eng.* **124**, 214 (2002).

46. A. Gefen, *Cellular and biomolecular mechanics and mechanobiology* (2012).

47. K. Imamura, T. Takeshima, Y. Kashiwaya, K. Nakaso, K. Nakashima, D-??-hydroxybutyrate protects dopaminergic SH-SY5Y cells in a rotenone model of Parkinson's disease. *J. Neurosci. Res.* **84**, 1376–1384 (2006).

48. J. Kovalevich, D. Langford, Considerations for the Use of SH-SY5Y Neuroblastoma Cells in Neurobiology. *Methods Mol. Biol.* **1078**, 9–21 (2013).

49. M. M. Shipley, C. A. Mangold, M. L. Szpara, Differentiation of the SH-SY5Y Human Neuroblastoma Cell Line. *J. Vis. Exp.*, 53193 (2016).

50. R. Constantinescu, A. T. Constantinescu, H. Reichmann, B. Janetzky, Neuronal differentiation and long-term culture of the human neuroblastoma line SH-SY5Y. *J Neural Transm*, 17–28 (2007).

51. Garrondo, Alzheimer's disease brain comparison. *Wikimedia Commons* (2008), (available at https://commons.wikimedia.org/wiki/File:Alzheimer%27s_disease_brain_comparison.jpg).